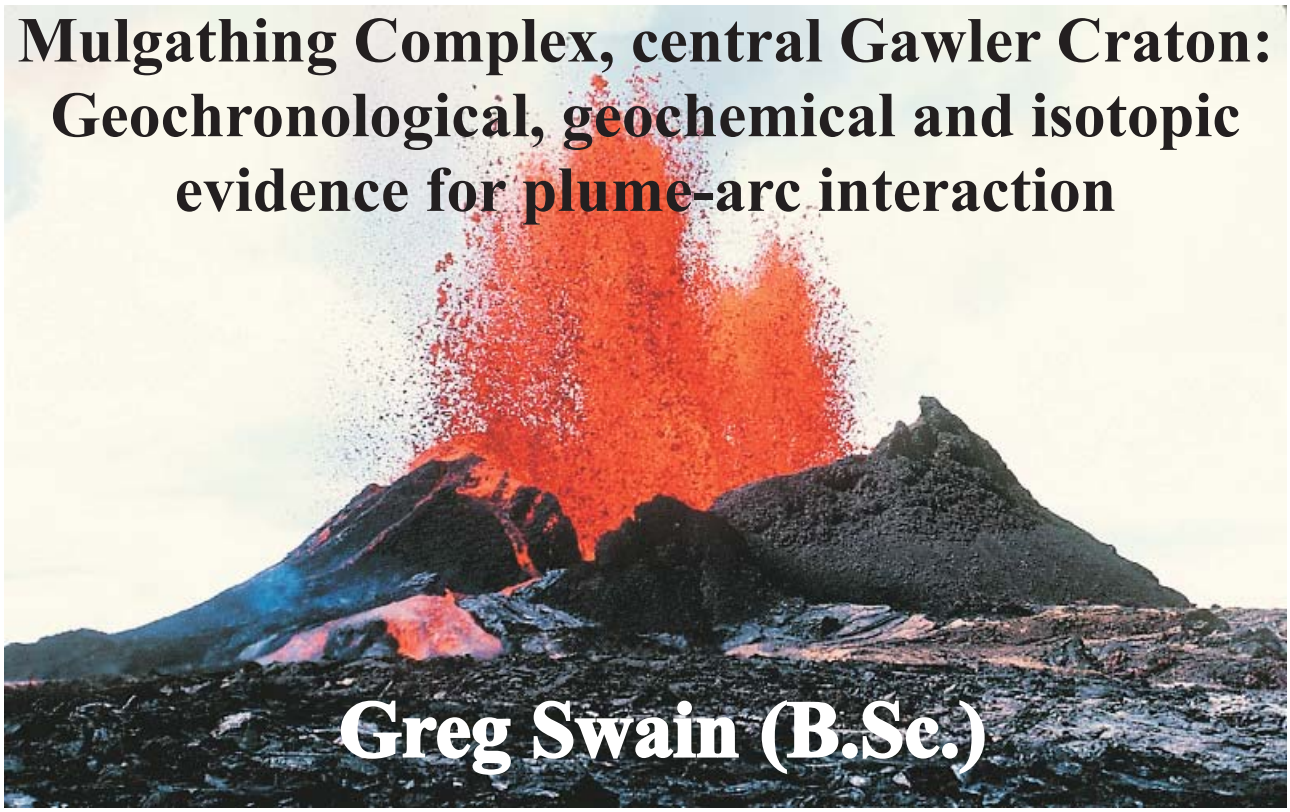
THE UNIVERSITY
OF ADELAIDE
AUSTRALIA

Provenance and tectonics of the late Archaean Mulgathing Complex, central Gawler Craton: Geochronological, geochemical and isotopic evidence for plume-arc interaction



Greg Swain (B.Se.)

Date: 11th day of November, 2002

Continental Evolution Research Group
University of Adelaide

PRIMARY INDUSTRIES AND RESOURCES SA

This paper is submitted as partial fullfilment for the
Honours degree of Bachelor of Science in Geology

Table of Contents

Table of Contents……1
List of Tables……2
List of Figures……2
Abstract……3
1. Introduction……4
2. Geological setting……5
3. Sampling and analytical methods……6
4. Results
4.1 SHRIMP zircon U-Pb isotopic results……7
4.1.1 Kenella Gneiss: sample 494305, 494306……8
4.1.2 LHGB metasedimentary rock: sample 495628……8
4.1.3 LHGB volcaniclastic rock: sample 495643……9
4.2 Geochemical results……9
4.3 Sm-Nd isotopic results……10
5. Discussion
5.1 Zircon U-Pb isotopic depositional age constraints and provenance……10
5.2 Geochemical constraints on provenance……11
5.3 Isotopic constraints on provenance……13
5.4 Tectonic implications for the late Archaean development of the Gawler Craton……14
6. Conclusion……17
Acknowledgements……18
References……18
Appendix 1
Metamorphic relationships……24
Appendix 2
Sample lithologies and locations……25

List of Tables

Table 1……...26
Table 2……...27
Table 3……...28
Table 4……...29
Table 5……...30
Table 6……...31

List of Figures

Figure Captions……32
Figure 1……34
Figure 2……35
Figure 3……36
Figure 4……37
Figure 5……38
Figure 6……39
Figure 7……40
Figure 8……41
Figure 9……42
Figure 10……43
Figure 11……44
Figure 12……45
Figure 13……46
Figure 14……47
Figure 15……48
Figure 16……49
Figure 17……50
Figure 18……50
Figure 19……51

Provenance and tectonics of the late Archaean Mulgathing Complex, central Gawler Craton: Geochronological, geochemical and isotopic evidence for plume-arc interaction

Greg Swain

Geology and Geophysics, School of Earth and Environmental Sciences
University of Adelaide, Adelaide

Abstract

Geochemical and Sm-Nd and U-Pb zircon isotopic data from late Archaean metasedimentary rocks of the Mulgathing Complex in the central Gawler Craton, South Australia, point to a dominance of late Archaean source terrains. Detrital zircon age data from the Kenella Gneiss are dominated by *ca*. 2700, 2600 and 2560 Ma age groups and the bulk rock composition shows uniform HREE depletion ($(La/Yb)_n$ = 76-17), suggesting a felsic volcanic and/or granitic source. Nd depleted mantle model ages (T_{DM}) between *ca*. 3000-2800 Ma are older than the bulk of the detrital zircon ages, suggesting that the protoliths to the Kenella Gneiss were derived from sources dominated by crustal reworking processes as opposed to first cycle sources dominated by juvenile material. In contrast to the Kenella Gneiss, the Christie Gneiss metapelites have flatter REE patterns ($(La/Yb)_n$ = 29-3), but a similar range of T_{DM} ages, suggesting a greater mafic component in their provenance. Metasediments and volcaniclastics associated with the komatiite-bearing Lake Harris Greenstone Belt (LHGB) are dominated by flat REE patterns ($(La/Yb)_n$ = 15-10) pointing to a significant mafic input, consistent with the presence of interlayered mafic and ultramafic rocks. Detrital zircons in the LHGB metasedimentary and volcaniclastic rocks range down to *ca*. 2505 Ma. These data, combined with existing U/Pb age constraints for cross cutting felsic rocks within the greenstones, indicate that the LHGB sequence was deposited at *ca*. 2505 Ma. This age is analogous to the youngest zircons in the Devil's Playground Volcanics, which are a sequence of Nb- and Ti-depleted felsic to intermediate volcanics in the NE Gawler Craton. This suggests that the LHGB sequence may be been deposited synchronously with eruption of the Devil's Playground Volcanics. Conceivably, the late Archaean sequences now preserved in the central Gawler Craton were deposited in an evolving back-arc style setting in which the Devil's Playground Volcanics represent felsic arc volcanism, and the LHGB localised mantle-plume associated rift development within the broader basin that contained the protolithic

sequences to the Kenella and Christie gneisses, deposited between *ca*. 2535-2510 Ma. Collisional closure of the back-arc system is recorded by the *ca*. 2500-2420 Ma Sleafordian Orogeny, which was associated with regional high geothermal gradient amphibolite-granulite grade metamorphism, an event recorded by extensive metamorphic zircon growth in the Kenella Gneiss and limited zircon growth in LHGB metasedimentary rocks.

Keywords: Archaean; Komatiite; Calc-alkaline; Plume; Subduction; Gawler Craton

1. Introduction

The Archaean was a period of major crustal growth during which various geological assemblages were collectively stabilized as cratonic terrains (Taylor and McLennan, 1985; Choukroune *et al*., 1997; Vogel *et al*., 1998; Henry *et al*., 2000). Granite-greenstone terrains dominate the late Archaean lithological association and comprise mafic-ultramafic and felsic volcanic, plutonic and metasedimentary rocks (Taylor and McLennan, 1985). Understanding the granite-greenstone lithological association and tectonic evolution of late Archaean cratons is fundamentally important as they host some of the most productive mineralized terrains worldwide (e.g. Swager and Nelson, 1997; Barley *et al*., 1998; Wyman *et al*., 1999).

Importantly, a significant number of late Archaean terrains have been recognized to evolve in a style akin to modern plate tectonic processes resulting in arc environments (e.g. Ayer and Davis, 1997; Champion and Sheraton, 1997; Barley *et al*., 1998; Hollings *et al*., 1999; Toulkeridis *et al*., 1999; Henry *et al*., 2000; Lahtinen, 2000; Lahtinen *et al*., 2002). Such an interpretation of Archaean rock systems supports the notion that modern continental growth processes played an important role in the Archaean. Within this context, recent studies have highlighted the contemporaneous existence of arc-related felsic volcanic rocks and plume-related komatiites, suggesting interaction between ascending mantle plumes and adjacent arc related subduction zones (e.g. Superior Province, Canada; Campbell *et al*., 1989; Xie *et al*., 1993; Dostal and Mueller, 1997; Hollings and Wyman, 1999; Hollings *et al*., 1999; Wyman *et al*., 1999; Polat and Kerrich, 2001). A number of studies have also demonstrated the importance of deciphering the record of provenance preserved in sedimentary rock systems (Taylor and McLennan, 1985; Maas and McCulloch, 1991; Lahtinen, 2000). The importance of understanding this record lies in the ability of sedimentary rocks and their metamorphosed equivalents to record geochemical and isotopic composition of older crust that has undergone erosion. In many instances, the sedimentary rock systems contain the only evidence for the existence of this older crust, and therefore hold important clues to the

compositions and evolution of Archaean proto cratons (e.g. Whitehouse *et al*., 1998; Lahtinen, 2000; Lahtinen *et al*., 2002)

This paper presents zircon U-Pb isotopic, geochemical and Sm-Nd isotopic data from late Archaean metasedimentary rocks of the Mulgathing Complex in the central Gawler Craton, southern Australia (Fig. 1). The study was undertaken to in order to determine the provenance of the late Archaean sequences, and to define a possible tectonic setting within which the sedimentary units accumulated. It forms part of a larger project involving the Continental Evolution Research Group at the University of Adelaide and the South Australian Office of Minerals and Energy Resources investigating the late Archaean evolution of the proto Gawler Craton.

2. Geological setting

The Mulgathing Complex (Fig. 2; Daly, 1985, 1986; Daly and Fanning, 1993; Daly *et al*., 1998) in the central Gawler Craton, southern Australia, is a poorly outcropping late Archaean terrain covering more than 6000 km^2. The recognized late Archaean lithologies from oldest to youngest include the Devil's Playground Volcanics, metaigneous/metasedimentary Kenella Gneiss, metasedimentary Christie Gneiss, Lake Harris Greenstone Belt (LHGB) which consists of mafic-ultramafic lavas, komatiites and interlayered metasedimentary rocks and the Glenloth Granite (Figs. 2, 3). The terrain has been affected by regional high grade Proterozoic tectonism associated with the *ca*. 2440 Ma Sleafordian Orogeny and *ca*. 1730 Ma Kimban Orogeny (Daly and Fanning, 1993; Daly *et al*., 1998).

The Devil's Playground Volcanics are a bimodal suite of calc-alkaline rhyodacite and andesite identified solely in drill hole 'Esso DP1' (Cowley and Fanning, 1992). The interpreted extrusive zircon U-Pb isotopic age from 9 grains is 2553±9 Ma (Fanning, 1997), while zircon U-Pb ages at *ca*. 2510 Ma from 4 grains are interpreted as possible intrusive effects of bodies such as the 2499±11 Ma Glenloth Granite (Fanning, 1997).

The Christie Gneiss, which principally outcrops near Mount Christie (Fig. 2), is a compositionally layered metasedimentary rock in which mesoscopic compositional layering reflects the original sedimentary sequence (Daly and Fanning, 1993). The metapelitic component is a coarse-grained granulite-grade gneiss predominantly composed of plagioclase, perthitic K-feldspar, quartz, garnet, cordierite, biotite and sillimanite, with leucosomes containing garnet and cordierite. A zircon U-Pb age of 2437±11 Ma (Fanning, 1997) is interpreted as recording peak granulite grade metamorphism during the Sleafordian Orogeny,

which has inferred peak pressure-temperature conditions of 4.5-5.5 kb and 750-800^{o}C (Teasdale, 1997). A maximum age for the deposition of the Christie Gneiss is yet to be determined, however the presence of Sleafordian-aged metamorphic zircon (Fanning, 1997) indicates that deposition must have occurred prior to 2437±11 Ma.

The Kenella Gneiss (Fig. 3) is a compositionally layered rock, consisting predominantly of perthitic feldspar, quartz, plagioclase, biotite and sillimanite and retrogressed garnets. Poor outcrop, limited drill-hole intersections and retrogression during the Kimban Orogeny (Daly *et al*., 1998) have hampered lithological interpretation for the Kenella Gneiss. The lithological association has been tentatively interpreted as metavolcanic, meta-igneous or metasedimentary (Daly and Fanning, 1993; Fanning 1997). At present there are no reliable age constraints for the timing of deposition of the protoliths to the Kenella Gneiss, but intrusion by the *ca*. 2500 Ma Glenloth Granite constrains its minimum age.

Ultramafic komatiites, basalts, pyroxenite and peridotite sills are all inferred to be contemporaneous with deposition of the Lake Harris Greenstone Belt (LHGB; Fig. 3; Daly *et al*., 1998; Zang *et al*., 2002). Interbedded with the komatiite flows are intervals of volcaniclastics, metasediments, and a 5m thick package of volcanic/volcaniclastics, chert and marble interval intruded by a rhyodacite dated at *ca*. 2500 Ma (Zang *et al*., 2002). The komatiite is intruded by the *ca*. 2500 Ma Glenloth Granite (Fanning, 1997; Zang *et al*., 2002). The lower to middle-amphibolite facies metamorphism of the LHGB (Zang *et al*., 2002) contrasts with granulite facies metamorphism of the adjacent Kenella and Christie gneisses.

The Glenloth Granite is the youngest identified component of the Mulgathing Complex, and ranges in composition from granite to granodiorite (Daly and Fanning, 1993). The body is poorly to well-foliated, medium to coarse-grained with an interpreted magmatic zircon U-Pb isotopic crystallization age of 2499±11 Ma (Fanning, 1997).

The aim of this study is to use zircon U-Pb, geochemical and Sm-Nd isotopic data to define the provenance of late Archaean rocks of the Mulgathing Complex, and to place them in a generalized stratigraphic context. Comparisons with other late Archaean terrains will aid in the application of a tectonic model for crustal development in the late Archaean Gawler Craton.

3. Sampling and analytical methods

Combined field and diamond drill core sampling was undertaken to obtain representative samples of the Kenella Gneiss, Christie Gneiss, LHGB metasedimentary and volcaniclastic rocks and the Glenloth Granite. Four samples were selected for U-Pb zircon

analyses. A suite of 21 samples were analyzed for whole rock, major, trace and rare earth element (REE) geochemistry. Of these, 10 samples were selected for Sm-Nd isotope analyses. Sample lithologies and locations are listed in Appendix 2.

Sensitive High Maas Resolution Ion Microprobe (SHRIMP) zircon U-Pb analyses were done using SHRIMP I at the Research School of Earth Sciences, Australian National University (ANU), Canberra. Choice of zircon grains and spots for analyses were obtained from transmitted/reflected light microscopy and cathodoluminescence (CL) imaging. Analytical techniques used in this study follow those given by Williams (1998). U-Pb data reduction was done using SQUID 1.02 (Ludwig, 2001) and age calculations were made using Isoplot/Ex rev. 2.49 (Ludwig, 2001).

Major, trace and REE geochemical analyses were done by AMDEL Laboratories, Adelaide. Major element oxides plus Cr, V, Sc and Zr were determined by Inductively Coupled Plasma-Optical Emission Spectroscopy (ICP/OES). Trace elements, including the REE's, were analyzed by Inductively Coupled Plasma-Maas Spectroscopy (ICP/MS).

Analytical techniques for whole rock Sm-Nd isotopic data have been detailed elsewhere (e.g. Foden *et al*., 1995). Samples were spiked with a ^{150}Nd-^{149}Sm, and digested in HF/HNO_3 in sealed high-pressure bombs for 4 days, evaporated in HCl, and sealed again in bombs overnight. Sm-Nd isotopic ratios were obtained by thermal ionization Maas spectrometry on a Finnigan MAT 262 Maas spectrometer at the University of Adelaide. Reproducibility is monitored by procedural analyses of an in house standard. The average for the in house standard is 0.511598±4 (2σ; *n*=23). The long term average for the La Jolla Nd standard is 0.511838±5 (2σ). Nd blanks ranged from 100 to 200 pg.

4. Results

4.1 SHRIMP zircon U-Pb isotopic results

SHRIMP zircon U-Pb isotopic data for zircons from Kenella Gneiss samples and LHGB metasedimentary and volcaniclastic rock samples which are stratigraphically bound by komatiites are presented in Tables 1 to 4, and displayed on concordia plots (Fig. 4). The data displayed on cumulative gaussian distribution/histogram plots (Fig. 5) has been filtered to 10% concordance and <2% common Pb (f206<2%) to avoid incorporation of zircon U-Pb isotopic data that had undergone either significant post or pre-depositional isotopic modification. Cathodoluminescence (CL) images of selected zircons from the four sample sets are shown in Figs 6, 7, 9 and 10

Since the main focus of the zircon U-Pb isotopic analyses was to determine the dominant age population for detrital zircons, analyses were largely from the cores of grains. However, some analyses of zircon overgrowths were done and are discussed in Appendix 1. Although zircon analyses from the LHGB metasediment (495628) are consistently discordant due to anomalously high common lead contents, only 18% of zircons from the two Kenella Gneiss samples showed greater then 5% discordance. Analyses to 10% discordance in Tables 1 to 4 are shown in bold.

4.1.1 Kenella Gneiss: samples 494305, 494306

Zircon U-Pb isotopic data from the two Kenella Gneiss samples 494305 and 494306 are presented in Tables 1 and 2. While both samples show broad population spreads, they display dominant peaks at *ca.* 2700-2650 and *ca.* 2600-2560 Ma (Fig. 5a, b). CL images (Figs. 6, 7) show that the *ca.* 2600-2560 Ma zircons are mainly euhedral and display igneous growth zoning while the *ca.* 2700-2650 Ma zircons are less consistently euhedral and display a range of growth zone patterns. Zircon grains older than *ca.* 2700 Ma appear rounded to sub-rounded with simple zoning of light CL cores and dark CL rims. The youngest concordant analysis from the outer edge of an igneous-style zircon has an age of 2536±8 Ma (analyses 43.2, 494305, Fig. 6). Analysis 43.1 is from the core of the zircon and has a concordant age of 2544±6 Ma. Analyses from CL dark overgrowths yielded ages that ranged from *ca.* 2500-2420 Ma. Two near concordant analyses from zircons 24.1 and 30.1 in sample 494305 gave ages of 1747±24 Ma and 1729±10 Ma respectively. In general, younger analyses are characterized by low Th/U ratios ≤ 0.2 (Fig. 8).

4.1.2 LHGB metasedimentary rock: sample 495628

Zircon U-Pb isotopic data for the LHGB metasediment sample 495628 are presented in Table 3. Zircon morphologies are dominantly euhedral with igneous-style growth zoning (Fig. 9). However, analyses are hindered by anomalously high abundances of common lead resulting in large errors and discordance.

Zircons analyzed from the LHGB metasediment display a dominant population at *ca.* 2520 Ma (Fig. 5c), combined with fewer older but significantly more discordant zircons. CL images of *ca*. 2520 Ma and *ca*. 2580-2530 Ma zircons are shown in Fig. 9. The youngest near concordant igneous-style zircon has an age of 2506±15 Ma (analysis 57.1). Zircon analysis

23.1 gave a concordant age of 2492±27 Ma. Two other almost concordant zircons 28.1 and 59.1 yielded ages of 2493±28 Ma and 2493±22 Ma respectively.

4.1.3 LHGB volcaniclastic rock: sample 495643

Zircon U-Pb isotopic data for the LHGB volcaniclastic (495643) are presented in Table 4. Analyses from the core of igneous-style zircons (e.g. analyses 2.1, 4.1, 15.1; Fig. 10) are consistently older than analyses from the edges (e.g. analyses 5.1, 6.1, 7.1, 14.1; Fig. 10). Zircon ages cluster at *ca*. 2535, *ca*. 2520 and *ca*. 2510 Ma. The youngest concordant igneous-style zircon age is 2504±13 Ma from analysis 16.1 (Table 4, Fig. 10). Two near concordant analyses 12.1 and 18.1 give ages of 2473±25 Ma and 2425±7 Ma respectively.

4.2 Geochemical results

Major, trace and REE data for samples from the Kenella Gneiss, Christie Gneiss, LHGB metasedimentary and volcaniclastic rocks and the Glenloth Granite are presented in Table 5. Major and trace elements (MgO, TiO_2, Al_2O_3, Ni and Ti) are plotted in Fig. 11 and REE's in Fig. 12.

Apart from Kenella Gneiss field samples 505727 and 505728, there appears to be a significant distinction between higher Ni contents in the Christie Gneiss relative to the other units (Fig. 11c). Clear distinctions exist between the REE patterns for the Archaean metasedimentary rocks of the Mulgathing Complex. The Kenella Gneiss has relatively fractionated REE patterns (Fig. 12) with the majority of samples (excluding field samples 505727 and 505728) showing HREE depletion ($(Gd/Yb)_n$ ~3.2), as opposed to the Christie Gneiss which has comparatively flat HREE patterns ($(Gd/Yb)_n$ ~2). $(La/Yb)_n$ for the Kenella Gneiss ranges from 76-17 and is consistently higher than the other units whose ratios are commonly <30 (Fig. 13). Two samples of Christie Gneiss (506603 and 506598) display significant negative Eu anomalies.

The Glenloth Granite is a high-Ca (3.1% and 3.5% CaO) granite spanning a narrow compositional range of 68-73% SiO_2 (Table 5). It has high Al_2O_3 (16%), moderate to high Na_2O and moderate K_2O, Rb and Pb, characteristic of typical Archaean tonalite-trondhjemite-granodiorite suites (TTG's; Fig. 14). It displays a fractionated REE pattern (Fig. 12) with $(La/Yb)_n$ ratios of 20 and 38 (Fig. 13) and variable Eu anomalies.

4.3 Sm-Nd isotopic results

Sm-Nd isotopic data for samples of the Kenella Gneiss, Christie Gneiss, LHGB metasedimentary and volcaniclastic rocks and the Glenloth Granite are presented in Table 6 and plotted on a ε_{Nd} versus age diagram (Fig. 15). Existing data from the *ca*. 2560 Ma Devil's Playground Volcanics (Cowley and Fanning, 1992) are included (Table 6, Fig. 15).

Based on the youngest concordant detrital zircon at 2536±8 Ma in the Kenella Gneiss, and intrusive relationships of the *ca*. 2500 Ma Glenloth Granite, a depositional age of 2530 Ma has been assumed in calculation of initial ε_{Nd} values for the Kenella and Christie gneisses. Based on the cross cutting relationship with the *ca*. 2500 Ma Glenloth Granite and the youngest concordant apparently detrital zircons at 2506±15 and 2504±13 Ma, a depositional age of 2505 Ma has been assumed in calculation of initial ε_{Nd} values for the LHGB metasedimentary and volcaniclastic rocks. Initial ε_{Nd} values for the Kenella Gneiss and Christie Gneiss range from +0.6 to -1.8 and -1.8 to -3.3 respectively. Initial ε_{Nd} values for the LHGB metasedimentary and volcaniclastic rocks are -1.2 and -1.4 respectively. At a crystallization age of *ca*. 2500 Ma for the Glenloth Granite, its initial ε_{Nd} values are -0.1 and -0.2. At a crystallization age of 2558 Ma (Cowley and Fanning, 1992; *sufficient for this study*), ε_{Nd} values for the Devil's Playground Volcanics range from +2.6 to -1.1 (Cowley and Fanning, 1992).

Depleted mantle model ages for all rocks in this study range from *ca*. 3180-2800 Ma, and were calculated using the model of Goldstein (1984). The depleted mantle model ages for the Devil's Playground Volcanics range from *ca*. 3190-2720 Ma (Cowley and Fanning, 1992).

5. Discussion

5.1 Zircon U-Pb isotopic depositional age constraints and provenance

Detrital zircon ages from the Kenella Gneiss place a maximum age constraint on deposition of the protolith of ≤ 2536±8 Ma. This age was obtained from concordant age data from the outermost part of an igneous-zoned zircon from sample 494305 (analysis 43.2, Table 1, Fig. 6). However, a zircon overgrowth age of 2511± 6 Ma (494305, analysis 13.2, Fig. 6), is older than the accepted age of the Sleafordian Orogeny (Fanning, 1997; Daly et al., 1998), and suggest that deposition of the Kenella protoliths may be as young as ≤ *ca*. 2510 Ma. The minimum age for deposition of the Kenella Gneiss is constrained by the *ca*. 2500 Ma Glenloth

Granite which intrudes the Kenella Gneiss at Earea Dam Goldfield (Daly and Fanning, 1993). Provenance ages for the Kenella Gneiss are highlighted in the zircon histograms (Fig. 5a, b) and display detrital zircon populations from *ca.* 2600-2530 Ma and from *ca.* 2700-2650 Ma. Older less abundant zircons in the Kenella Gneiss indicate a more mature and/or recycled provenance input.

The Kenella Gneiss does not contain the *ca*. 2530-2500 Ma detrital zircons found in the LHGB samples (Fig. 5). This suggests that either (1) the Kenella Gneiss may have originally been basement to the LHGB, or that (2) it forms part of a roughly coeval depositional system that was isolated from the LHGB. The first suggestion is favored on the basis that *ca*. 2700, 2650 and 2600 Ma detrital zircon input into the LHGB metasediments is consistent with detrital zircon signatures found in the Kenella Gneiss.

The youngest concordant detrital zircon age from the LHGB metasediment is 2506±15 Ma (analysis 57.1, Table 3, Fig. 9). Similarly, the youngest concordant zircon age from the LHGB volcaniclastic is 2504±13 Ma (analysis 16.1, Table 4, Fig. 10). The LHGB metasediment and volcaniclastic rocks are bounded by komatiitic lava flows. Subsequent intrusion by the *ca*. 2500 Ma Glenloth Granite implies that the LHGB was formed at *ca*. 2505 Ma. This age is essentially identical to the youngest zircons in the Devil's Playground Volcanics (Fanning, 1997). If the *ca*. 2510 Ma zircons in the Devil's Playground Volcanics record the extrusive age of the volcanics, (as opposed to intrusive effects of the *ca*. 2500 Ma Glenloth Granite; Fanning, 1997), they point to a synchronicity of felsic volcanism with the development of the LHGB. LHGB metasediment is dominated by zircons aged from *ca.* 2540-2505 Ma (Table 3, Fig. 5c) which display oscillatory growth zoning (Fig. 9). Older inherited zircons range in age from *ca*. 2700-2650 Ma, suggesting erosion of a similar source to the Kenella Gneiss. Zircons in LHGB volcaniclastics display oscillatory growth zoning and have ages that cluster between *ca.* 2520-2505 Ma. CL morphologies and the age cluster of these volcaniclastic hosted zircons are suggestive of felsic igneous activity, conceivably related to volcanic venting and ash deposition.

5.2 Geochemical constraints on provenance

Due to potential disturbance of the major elements by high-grade metamorphism during the *ca*. 2440 Ma Sleafordian and *ca*. 1730 Ma Kimban Orogeny, geochemical appraisal of the sequences focuses on immobile trace and REE to constrain sources (e.g. Xie *et al*., 1993; Hollings and Wyman, 1999; Hollings *et al*., 1999). However, it is necessary to evaluate the impact that fluid-absent partial melting may have played in changing the

sedimentary trace and REE compositions. Mineral assemblages preserved in the Kenella and Christie Gneisses are consistent with metamorphic conditions of around 750-800^{o}C and 4.5-5.5 kbar (Appendix 1; Teasdale, 1997; White *et al*., 2001). Within these metamorphic rocks, particularly the Christie Gneiss, the preservation of near anhydrous garnet-bearing metamorphic granulite assemblages requires substantial extraction of melt during peak metamorphism (White et al., 2001). The preservation of 10-25 volume % garnet preserved in these metapelitic rocks at conditions of 750-800^{o}C and 4.5-5.5 kbar (Teasdale, 1997) would require around 30-40 volume % melt extraction (Schnetger, 1994; White *et al*., 2001), leading to significant volume reduction of the system.

A number of studies (e.g. Sighinolfi and Gorgoni, 1978; Schnetger, 1994) have shown that trace elements such as Sc, V, Ni, Cr can increase significantly (by factors ~2) across amphibolite to granulite transitions, effectively due to the compatibility of these elements in granulitic minerals such as garnet which remain in the granulitic residue after melt extraction (30-40 volume %; White *et al*., 2001) has occurred. This suggests that relative changes in trace element concentrations of ≤ 2 between sequences subjected to large scale partial melting and melt extraction, and those that did not undergo melting, should not be used as a basis for proposing different sedimentary source rock ratios.

A number of studies have also shown that the bulk of the REE budget in amphibolite-grade metasediments is contained in monazite, which is dominated by the LREE, and to a lesser extent xenotime, which is essentially the only mineral containing high HREE concentrations (e.g. Bea, 1996; Bingen *et al*., 1996; Bea and Montero, 1999). The behavior of monazite and xenotime during amphibolite to granulite transition is therefore crucial in determining whether partial melting affects the REE composition of rocks. The low solubility of monazite in melt (e.g. Rapp and Watson, 1986; Montel, 1993; Wolf and London, 1995) means that the modal abundance of monazite in the rock across the amphibolite to granulite transition does not change significantly (e.g. Bea and Montero, 1999). Partly this is because the fraction of monazite lost via melt extraction is approximately compensated by the volume reduction associated with loss of melt from the system (e.g. Schnetger, 1994; Bea and Montero, 1999). In contrast to the stability of monazite in granulite grade rocks, fluid-absent partial melting is marked by decreases in the abundance of xenotime (e.g. Wolf and London, 1995), attributed to its consumption in garnet-producing reactions (Bea and Montero, 1999). This means that the HREE budget in xenotime is redistributed during partial melting, but retained in the garnet restitic portion (e.g. Bea and Montero, 1999).

The foregoing argument suggests that the REE budget of metasedimentary rocks of the Mulgathing Complex can be used as reasonably reliable indicators of sediment provenance (e.g. Taylor and McLennan, 1985; Rollinson, 1993; Bea and Montero, 1999).

The REE characteristics for the majority of samples from the Mulgathing Complex are typical of Archaean sediments in that they have no significant Eu-anomalies (Fig. 12). HREE depletion in the metasedimentary rocks ($(La/Yb)_n$ consistently > 10) probably reflect a dominantly felsic volcanic and/or plutonic source (Taylor and McLennan, 1985; Maas and McCulloch, 1991; Rollinson, 1993). The less fractionated REE pattern of the Christie Gneiss relative to the Kenella Gneiss (Fig. 12) would imply that 30-50 volume % mafic component would need to be mixed with a felsic volcanic and/or granitic source (e.g. Taylor and McLennan, 1985). Maas and McCulloch (1991) suggested that rather than having a 30-50 volume % mafic component, high Cr and Ni abundances in pelitic rocks could be derived from small (<10%) proportions of ultramafic material added to a predominantly felsic, K-rich detritus. Average Ni content in the Christie Gneiss (~42 ppm Ni) compared to the Kenella Gneiss (~6 ppm Ni, excluding field samples 505727 and 505728) is consistent with a <10% ultramafic source input. Consistently lower $(La/Yb)_n$ of the Christie Gneiss (predominantly ≤ 30 as opposed to 76-17 for the Kenella Gneiss; Fig. 13) represents a less fractionated REE pattern, consistent with a mafic/ultramafic input (Taylor and McLennan, 1985; Rollinson, 1993).

5.3 Isotopic constraints on provenance

Depleted mantle model ages (T_{DM}) at an assumed depositional age of 2530 Ma for the Kenella Gneiss and Christie Gneiss range between *ca*. 3000-2800 Ma and *ca*. 3180-2950 Ma respectively (Table 6, Fig. 15), indicating input from a mature late Archaean source. The depleted mantle model ages for the LHGB metasedimentary and volcaniclastic rocks (2915 and 2947 Ma respectively), suggest that *ca*. 2540-2505 Ma igneous activity, highlighted in the zircon populations, was the result of partial melting and/or mixing of older crustal material.

Amid partial melting and recycling of older crust, components of the Devil's Playground volcanics indicate a mantle signature with ε_{Nd} values as primitive as +2.6 (T_{DM} model age of 2720 Ma; Cowley and Fanning, 1992). It is not improbable that the *ca*. 2560 Ma component in the Devil's Playground Volcanics represents a source that may have partly contributed felsic detrital material to the Kenella Gneiss sedimentary protoliths which have depleted mantle model ages between *ca.* 2800-2870 Ma. The *ca*. 3100-3000 and/or 2700 Ma

source component, as recorded in the detrital zircon signatures and Nd depleted mantle model ages for rocks of the Mulgathing Complex, is yet to be located in the Gawler Craton.

Correlation of geochronological, metamorphic and magmatic histories in basement rocks exposed on the Eyre Peninsula, southern Gawler Craton and Terre Adélie Land, Antarctica, have been used to propose the existence of a juvenile craton called the 'Mawson Continent' (Fig. 16; Fanning *et al*., 1995, 1996, 2002). Importantly, low-grade rocks from Cape Hunter in Terre Adélie contain *ca*. 2500 Ma detrital zircons (Oliver and Fanning, 1997), suggesting an affinity with the metasediments of the Mulgathing Complex. The Archaean rocks exposed in Terre Adélie Land form part of an apparently large Archaean province in Antarctica (Fig. 16). Within this province, rocks of the Nimrod Group in the central Transantarctic Mountains, Antarctica, reveal U-Pb evidence for igneous growth of euhedral zircons at *ca*. 3100 to 3000 Ma (Bennett and Fanning, 1993; Goodge and Fanning, 1999; Goodge *et al*., 2001), igneous events at *ca*. 2900 and 2500 Ma (Goodge and Fanning, 1999) and zircons with oscillatory growth zoning at 2675 Ma (Goodge *et al*., 2001). Nd model ages for the rocks of the Nimrod Group range between *ca*. 3100-2710 Ma (Borg *et al*., 1990; Borg and DePaolo, 1994). The geochronological and isotopic similarity between major rock forming events in the Nimrod Group and the similarity of detrital zircon signatures in the Gawler Craton and Terre Adélie Land metasedimentary rocks suggest that Archaean rocks that were once and/or still located between Terre Adélie Land and the Nimrod Group were a source for late Archaean sediments in the Gawler Craton.

5.4 Tectonic implications for the late Archaean development of the Gawler Craton

The origin of Archaean greenstone belts such as the LHGB, has long been the focus of debate (e.g. Arndt, 1994; Dostal and Mueller, 1997; Polat and Kerrich, 2001, 2002). Komatiitic and felsic volcanic rock associations have been well documented in the Superior Province and other Archaean cratons (Barley *et al*., 1998; Hollings *et al*., 1999; Wyman *et al*., 1999; Polat and Kerrich, 2001), and have been used to define the processes of terrain development (e.g. Dostal and Mueller, 1997). In this context, a comparison between the geochemical signatures of the Devil's Playground Volcanics (Cowley and Fanning, 1992), LHGB komatiitic lavas (MER data, in prep) and the Glenloth Granite with equivalent rocks from other Archaean cratons may serve as a useful starting point from which to development tectonic models for the late Archaean Gawler Craton.

The presently poorly understood calc-alkaline Devil's Playground Volcanics (Fig. 2) may be an integral part of the late Archaean Mulgathing Complex. These little deformed or

metamorphosed volcanics have an interpreted U-Pb crystallization age of 2553±9 Ma (Fanning, 1997), based on 9 analyses from a total of 13. The remaining 4 analyses have ages around 2510 Ma, which were attributed to the thermal effects of the *ca*. 2500 Ma Glenloth Granite (Fanning, 1997). However, it is also possible the *ca.* 2510 Ma zircons represent the crystallization age of the volcanics, with the *ca*. 2560 Ma zircons representing an inherited component. The suggestion that the Devil's Playground Volcanics contains inherited late Archaean crustal material is supported by Nd isotopic data (Cowley & Fanning, 1992; Fig. 15) which requires a component of older crustal material. Viewed in this context it is suggested here that 2510 Ma is the crystallization age for the calc-alkaline Devil's Playground Volcanics.

The geochemical signature of the Devil's Playground Volcanics is highlighted by strong depletions in Nb and Ti, which coupled with Nd evidence for crustal contamination in the majority of samples (Cowley and Fanning, 1992), has the hallmarks of subduction related arc-type felsic volcanics such as those documented in the late Archaean Superior Province, Canada (Fig. 17).

Although slightly younger than the Devil's Playground Volcanics, the 2500 Ma Glenloth Granite may also point to subductive processes in the tectonic evolution of the late Archaean Gawler Craton. The Glenloth Granite is compositionally similar to tonalite-trondjemite granites (TTG) from other late Archaean cratons (Fig. 14; e.g. Eastern Goldfields, Yilgarn Craton). Champion and Sheraton (1997) show that high-Ca granites in the Yilgarn Craton appear to have been derived at high pressures by partial melting of mafic to intermediate source (e.g. subducted oceanic crust) or remelting of an older source derived by such processes. TTG suites have been interpreted to show similarities to Cenozoic subduction-related felsic adakites, implying subduction style tectonics existed in Archaean terrains (Defant and Drummond, 1990; Drummond and Defant, 1990).

The association of komatiitic sequences intercalated with felsic volcanic rocks (e.g. Abitibi and northern Superior Province, Canada; Norseman-Wiluna Belt, Yilgarn Craton) is increasingly being interpreted as reflecting interaction between an ascending mantle-plume and adjacent subduction zones (Barley *et al*., 1998; Hollings *et al*., 1999; Wyman *et al*., 1999; Polat and Kerrich, 2001). Although considerable effort has been expended on studying the genesis of komatiites (e.g. Campbell *et al*., 1989; Arndt, 1994) the geodynamic environments proposed for komatiite generation remains enigmatic. However, two distinctly different general tectonic settings are thought to be important in their formation: (1) rifting of a stable continental landmass (e.g. Belingwe Greenstone Belt, Zimbabwe Craton; Bickle and Nisbet, 1993; Bickle *et al*., 1994), and (2) rifting of oceanic lithosphere (Dupre *et al*., 1984; de Wit *et*

al., 1987; Dostal and Mueller, 1997). Campbell *et al* (1989) argue that komatiites originated from mantle melts transported by upwelling mantle plumes, consistent with temperatures of ~1500^{o}C which are required to produce melts with ≥ 30 wt% MgO (Hill *et al*., 1990). Geochemical signatures including negative Zr and Hf anomalies in the LHGB komatiites (MER data, in prep) are consistent with plume-related komatiites documented in the Red Lake and Lumby Lake greenstone belts (Hollings and Wyman, 1999; Hollings *et al*., 1999), Abitibi Greenstone Belt (Dostal and Mueller, 1997) of the Superior Province (Fig. 18), and in komatiites from the Kolar Schist Belt, India (Rajamani *et al*., 1995). The proximal association of basalts and komatiites within the LHGB (Daly and Fanning, 1993; Fanning, 1997) also occurs in the above terrains, and is consistent with melts derived from extrusion of magma sourced from a cool part of the plume head (Dostal and Mueller, 1997).

The presence of the arc-style calk-alkaline Devil's Playground Volcanics, and the TTG-style Glenloth Granite in the central Gawler Craton, coupled with mantle-plume related LHGB komatiites, is consistent with possible impingement of a mantle-plume on an arc-related terrain undergoing active subduction. The tectonic model proposed for the evolution of the late Archaean Gawler Craton at *ca*. 2510-2505 Ma (Fig. 19) is consistent with the style of tectonic evolution documented in many other late Achaean terrains; e.g. Abitibi Subprovince (Dostal and Mueller, 1997; Wyman *et al*., 1999; Polat and Kerrich, 2001, 2002), Lumby Lake Greenstone Belt (Hollings and Wyman, 1999), Northern Superior Province (Hollings *et al*., 1999) of the Superior Province, Canada; Kolar Schist Belt, India (Rajamani *et al*., 1995); ~2100 Ma Birimian terrains of West Africa (Boher *et al*., 1992).

Prior to the *ca*. 2510 Ma volcanism of the Devil's Playground Volcanics and the LHGB mafic and ultramafic lava (Fig. 19), an envisaged back-arc shallow marine depositional environment is consistent with the interlayered banded iron formation, carbonates and calcsilicates identified in the Christie Gneiss (Daly and Fanning, 1993). Older Nd depleted mantle model ages recorded in the Christie Gneiss (T_{DM} *ca*. 3200-2970 Ma) as opposed to the Kenella Gneiss (T_{DM} *ca*. 3000-2800 Ma) suggests that the protoliths to the Christie Gneiss may have been a comparatively early deposited sedimentary sequence predominantly sourcing felsic and mafic/ultramafic material from mature late Archaean continental crust. Geochemical and Sm-Nd and U-Pb isotopic characteristics of the Kenella Gneiss metasedimentary package suggest input from both (1) increased felsic detritus sourced from a young arc composed of recycled crust (T_{DM} *ca*. 3000-2800 Ma; U-Pb *ca*. 2700-2650Ma and *ca*. 2600-2560 Ma), and (2) material sourced from the mature continental crust similar to the Christie Gneiss protolith (U-Pb *ca*. 3000 Ma; Fig. 5).

The cessation of further deposition of sedimentary protoliths to the Kenella Gneiss at ≤ 2530 Ma is suggested by the absence of detrital zircons younger than this age. The presence of detrital zircons as young as *ca*. 2505 Ma in sediments and volcaniclastics associated with the LHGB mafic and ultramafic lavas, and the inferred presence of *ca*. 2510 Ma volcanism represented by the Devil's Playground Volcanics, suggests that the basin may have been blanketed by volcanism and volcanic-derived sediments around that time (Fig. 19).

In the envisaged tectonic regime (Fig. 19), the thinned lithosphere within the back-arc basin would have been characterized by high heat flow, creating a system sensitive to thickening if the regime became collisional. A collisional regime could arise simply by shallowing of the subduction angle (e.g. Collins, 2002). Importantly, the generation of a collisional regime within the context of on-going subduction allows the possibility of a long-lived collisional system (e.g. Eriksson *et al*., 2001; Karlstrom *et al*., 2001), and also allows deposition in the back arc to continue up until orogenesis gets underway. This may offer an explanation for (1) the apparent near overlap of depositional age of sequences such as the LHGB metasediments and the onset of the Sleafordian Orogeny and (2), the apparently long-lived nature of the Sleafordian Orogeny during which metamorphic zircon growth appears to have occurred over the interval *ca*. 2500-2420 Ma (Fanning, 1997; Daly et al., 1998).

6. Conclusion

Nd depleted mantle model ages (T_{DM}) and detrital zircon U-Pb data indicate that the protoliths to late Archaean metasedimentary rocks from the Mulgathing Complex in the central Gawler Craton are derived from late Archaean crust. T_{DM} for the Christie and Kenella gneisses ranges between 3200-2800 Ma. This is 100-300 Ma older than the bulk of the detrital zircons in the sequences, and points to erosion of crustal reservoirs that were undergoing recycling comparatively soon after bulk extraction from the mantle.

Geochemical and REE data indicates somewhat contrasting provenances for the different sequences. The Kenella Gneiss shows uniform HREE depletion ($(La/Yb)_n$ = 76-17), suggesting derivation largely from a felsic volcanic and/or granitic source. In contrast, metapelitic rocks belonging to the Christie Gneiss and metasediments interlayered with mafic and ultramafic flows in the Lake Harris Greenstone Belt have flatter REE patterns ($(La/Yb)_n$ <30), consistent with a greater mafic/ultramafic component in the provenance.

On the basis of minimum detrital zircons ages and ages of cross cutting granites, the Lake Harris Greenstone Belt is interpreted to have been deposited at *ca*. 2505 Ma. It represents the youngest of the Archaean sequences in the central Gawler Craton and was

deposited in a rift-style setting on a basement that included the protoliths to the Kenella and Christie gneisses. Extrusion of mafic and ultramafic lavas within the Lake Harris Greenstone Belt at *ca*. 2505 Ma appears to have been synchronous with the eruption of the arc-like calc-alkaline Devils Playground Volcanics. A tectonic regime involving the on-going evolution of a back arc system is envisaged to explain both the depositional environment for the late Archaean sequences, and the subsequent development of the long-lived Sleafordian Orogeny, which affected most of the late Archaean Gawler Craton.

Acknowledgements

I would like to extend many thanks to my supervisors Dr Martin Hand and Dr Karin Barovich for much needed inspirational support and constructive criticism during this project. Many thanks are also extended to Michael Schwarz and his fellow Gawler Craton team from The Office of Minerals and Energy Resources, South Australia, who provided significant financial and intellectual assistance. Acknowledgement is also given to M. Fanning for proving time to use the SHRIMP facilities at RSES, Australian National University, Canberra.

References

Arndt, N.T., 1994. Archaean komatiites. In Condie, K.C., ed., Archaean Crustal Evolution: Amsterdam, Elsevier, p 11-44.

Ayer, J.A., Davis, D.W., 1997. Neoarchean evolution of differing convergent margin assemblages in the Wabigoon Subprovince: geochemical and Geochronological evidence from the Lake of the Woods greenstone belt, Superior Province, Northwestern Ontario. Precambrian Res., 81: p 155-178.

Barley, M.E., Krapez, B., Groves, D.I., Kerrich, R., 1998. The late Archaean bonanza: metallogenic and environmental consequences of the interaction between mantle plumes, lithospheric tectonics and global cyclicity. Precambrian Res., 91, p 65-90.

Bea, F., 1996. Residence of REE, Y, Th and U in granites and crustal protoliths: Implications for the chemistry of crustal melts. Journal of Petrology, 37: p 521-552.

Bea, F., Montero, P., 1999. Behaviour of accessory phases and redistribution of Zr, REE, Y, Th, and U during metamorphism and partial melting of metapelites in the lower crust: An example from the Kinzigite Formation of Ivrea-Verbano, NW Italy. Geochim. Cosmochim. Acta, 63: p 1133-1153.

Beaumont, C., Ellis, S., Hamilton, J., Fullsack, P., 1996. Mechanical model for subduction-collision tectonics of alpine-type compressional orogens. Geology, 24; 8: p 675-678.

Bennett, V.C., Fanning, C.M., 1993, A glimpse of the cryptic Gondwana shield: Archaean and Proterozoic ages from the central Transantartic Mountains. Geological Society of America, Abstracts with Programs 25: p 49.

Bickle, M.J., Nisbet, E.G., 1993. The geology of the Belingwe greenstone belt, Zimbabwe. Geol. Soc. Zimbabwe Spec. Pub. 2: p 238.

Bickle, M.J., Nisbet, E.G., Martin, A., 1994. Archaean greenstone belts are not oceanic crust. Journal of Geology, 102: p 121-138.

Bingen, B., Demaiffe, D., Hertogen, J., 1996. Redistribution of rare earth elements, thorium, and uranium over accessory minerals in the course of amphibolite to granulite facies metamorphism: The role of apatite and monazite in orthogneisses from southwestern Norway. Geochim. Cosmochim. Acta, 60: p 1341-1354.

Borg, S.G., DePaolo, D.J., 1994. Laurentia, Australia, and Antartica as a Late Proterozoic supercontinent: constraints from isotopic mapping. Geology, 22: p 307-310.

Borg, S.G., DePaolo, D.J., Smith, B.M., 1990. Isotopic structure and tectonics of the central Transantarctic Mountains. J. of Geophys. Res., 95: p 6647-6669.

Boher, M., Abouchami, W., Michard, A., Albarede, F., Arndt, N.T., 1992. Crustal growth in West Africa at 2.1 Ga. J. of Geophys. Res., 97: p 345-369.

Campbell, I.H., Griffiths, R.W., Hill, R.I., 1989. Melting in an Archaean mantle plume: Heads it's basalts, tails it's komatiites. Nature, 339: p 697-699.

Champion, D.C., Sheraton, J.W., 1997. Geochemistry and Nd isotope systematics of Archaean granites of Eastern Goldfields, Yilgarn Craton, Australia: Implications for crustal growth processes. Precambrian Res., 83: p 109-132.

Choukroune, P., Ludden, J.N., Chardon, D., Calvert, A.J., Bouhallier, H., 1997. Archaean crustal growth and tectonic processes: a comparison of the Superior Province, Canada and the Dharwar Craton, India. Orogeny Through Time, Geol. Soc. Special Publication, 121: p 63-98.

Collins, W.J., 2002. Nature of extensional accretionary tectonics. Tectonics, 21.

Cowley, W.M., Fanning, C.M., 1992. Low-grade Archaean Metavolcanics in the northern Gawler Craton. The Geological Survey of South Australia, Quarterly Geological Notes, 119: p 2-17.

Defant, M.J., Drummond, M.S., 1990. Derivation of some modern arc magmas by melting of young subducted lithosphere. Nature, 347: p 662-665.

de Wit, M.J., Hart, R.A., Hart, R.J., 1987. The James-town ophiolite complex, Barberton Mountain belt: A section through 3.5 Ga oceanic crust. J. Afr. Earth Sci., 6: p 681-730.

Drummond, M.S., Defant, M.J., 1990. A model for Trondhjemitic-tonalitic-dacite genesis and crustal growth via slab melting: Archaean to modern comparisons. J. of Geophys. Res., 95: p 21503-2152.

Daly, S.J., 1985. TARCOOLA map sheet. South Australia. Geological Survey. 1:250 000 series, sheet SH53-10.

Daly, S.J., 1986. The Mulgathing Complex. South Australia. Department of Mines and Energy. Report Book, 86: p 41.

Daly, S.J., Fanning, C.M., 1993. Archaean. In: Drexel, J.F., Preiss, W.V., Parker, A.J. (editors), The Geology of South Australia. Vol.1, The Precambrian. Geological Survey of South Australia, Bulletin 54.

Daly, S.J., Fanning, C.M., Fairclough, M.C., 1998. Tectonic evolution and exploration potential of the Gawler Craton, South Australia. AGSO J. of Australian Geology and Geophysics, 17(3): p 145-168.

Dostal, J., Mueller, W.U., 1997. Komatiite Flooding of a Rifted Archaean Rhyolitic Arc Complex: Geochemical Signature and Tectonic Significance of the Stoughton-Roquemaure Group, Abitibi Greenstone Belt, Canada. The Journal of Geology, 105: p 545-563.

Dupre, B., Chauvel, C., Arndt, N.T., 1984. Pb and Nd isotopic study of two komatiite flows from Alexo, Ontario. Geochim. Commochim. Acta, 48: p 1965-1972.

Eriksson, P.G., Altermann, W., Catuneanu, O., van-der-Merwe, R., Bumby, A.J., 2001. Major influences on the evolution of the 2.67-2.1 Ga Transvaal Basin, Kaapvaal Craton. In: Eriksson, P.G., Catuneanu, O., Aspler, L.B., Chiarenzelli, J.R., Martins, N.M.A., (Eds.), The influence of magmatism, tectonics, sea level change and paleo-climate on Precambrian basin evolution; change over time. Sedimentary Geology, 141-142; p 205-231.

Fanning, C.M., 1997. Geochronological synthesis of Southern Australia. Part II. The Gawler Craton. South Australia Department of Mines and Energy, Open File Envelope 8918 (unpublished).

Fanning, C.M., Moore, D.H., Bennett, V.C., Daly, S.J., 1996. The 'Mawson Continent': Archaean to Proterozoic crust in the East Antarctic Shield and Gawler Craton, Australia: A cornerstone in Rodinia and Gondwanaland. Geol. Soc. of Aust., Geol. Conv., 41: p135.

Fanning, C.M., Menot, R-P., Peucat, J.J., Pelletier, A., 2002. A closer examination of the direct links between southern Australia and Terre Adelie and George V Land, Antarctica. Abstract, 16th Australian Geological Convention, Abstracts Volume 67: p 224.

Fanning, C.M., Daly, S.J., Bennett, V.C., Menot, R.P., Peucat, J.J., Oliver, R.L., Monnier, O., 1995. The 'Mawson Block': once contiguous Archaean to Proterozoic crust in the East Antarctic Shield and Gawler Craton. VII International Symposium on Antarctic Earth Sciences, Siena, Italy: p 124.

Foden, J., Mawby, J., Kelley, S., Turner, S., Bruce, D., 1995. Metamorphic events in the eastern Arunta Inlier, part 2. Nd-Sr-Ar isotopic constraints. Precambrian Res., 71: p 207-227.

Goldstein, S., O'Noins, R.K., Hamilton, P.J., 1984. A Sm-Nd isotopic study of atmospheric dusts and particulates from major river systems. Earth Planet. Sci. Lett., 70: p 221-236.

Goodge, J.W., Fanning, C.M., 1999. 2.5 billion years of punctuated Earth history as recorded in a single rock. Geology, 27: p 1007-1010.

Goodge, J.W., Fanning, C.M., Bennett, V.C., 2001. U-Pb evidence of ~ 1.7 Ga crustal tectonism during the Nimrod Orogeny in the Transantarctic Mountains, Antartica: implications for Proterozoic plate reconstructions. Precambrian Res., 112: p 261-288.

Henry, P., Stevenson, R.K., Larbi, Y., Gariépy, C., 2000. Nd isotopic evidence for Early to Late Archean (3.4-2.7 Ga) crustal growth in the Western Superior Province (Ontario, Canada). Tectonophysics, 322: p 135-151.

Hill, R.E.T., Barnes, S.J., Gole, M.J., Dowling, S.E., 1990. The physical volcanology of Komatiites: a field guide to the Komatiites of the Norseman-Wiluna Greenstone Belt, Eastern Goldfields Province, Yilgarn Block, Western Australia. Geological Society of Australia, Excursion Guide Book No. 1: p 100.

Hollings, P., Wyman, D., 1999. Trace element and Sm-Nd systematics of volcanic and intrusive rocks from the 3 Ga Lumby Lake Greenstone belt, Superior Province: evidence for Archaean plume-arc interaction. Lithos, 46: p 189-213.

Hollings, P., Wyman, D., Kerrich, R., 1999. Komatiite-basalt-rhyolite volcanic associations in Northern Superior Province greenstone belts: significance of plume-arc interaction in the generation of the proto continental Superior Province. Lithos, 46: p 137-161.

Karlstrom, K.E., Ahall, K.I., Harlan, S.S., Williams, M.L., McLelland, J., Geissman, J.W., 2001. Long-lived (1.8-1.0 Ga) convergent orogen in southern Laurentia, its extensions to Australia and Baltica, and implications for refining Rodinia. In: Bartley, J.K., Kah, L.C., (Eds.,), Rodinia and the Mesoproterozoic Earth-ocean system. Precambrian Res., 111; 1-4: p 5-30.

Lahtinen, R., 2000. Archaean-Proterozoic transition: geochemistry, provenance and tectonic setting of metasedimentary rocks in central Fennoscanadian Shield, Finland. Precambrian Res., 104: p 147-174.

Lahtinen, R., Huhma, H., Kousa, J., 2002. Contrasting source components of the Paleoproterozoic Svecofennian metasediments: Detrital zircon U-Pb, Sm-Nd and geochemical data. Precambrian Res., 116: p 81-109.

Ludwig, K.R., 2001. User's manual for Isoplot/Ex, rev. Version 2.49, A Geochronological Toolkit for Microsoft Excel. Berkeley Geochronology Centre, Berkley, CA, Special Publication No. 1a.

Martin, H., 1994. The Archaean grey gneisses and the genesis of continental crust. In: Condie, K.C. (Ed.), Archaean Crustal Evolution. Elsevier, Amsterdam, p 205-259.

Maas, R., McCulloch, M.T., 1991. The provenance of Archaean metasediments in the Narryer Gneiss Complex, Western Australia: Trace element geochemistry, Nd isotopes, and U-Pb ages for detrital zircons. Geochim. Cosmochim. Acta, 55: p 1915-1932.

McDonough, W.F., Sun, S.S., 1995. The composition of the Earth. Chemical Geology, 120: p 223-254.

MER data, in prep. *Data obtained from* The Office of Minerals and Energy Resources, South Australia.

Montel, J.M., 1993. A model for monazite/melt equilibrium and the application to the generation of granitic magmas. Chemical Geology, 110: p 127-146.

Oliver, R.L., Fanning, C.M., 1997. Australia and Antarctica: Precise correlation of Palaeoproterozoic terrains. In: Ricci, C.A. (Ed.), The Antarctic Region: Geological Evolution and Processes. Terra Antarctica Publication, Siena: p 163-172.

Polat, A., Kerrich, R., 2000. Archaean greenstone belt magmatism and the continental growth-mantle evolution connection: constraints from Th-U-Nb-LREE systematics of the 2.7 Ga Wawa Subprovince, Superior Province, Canada. Earth and Planetary Science Letters, 175: p 41-54.

Polat, A., Kerrich, R., 2001. Geodynamic processes, continental growth, and mantle evolution in late Achaean greenstone belts of the Southern Superior Province, Canada. Precambrian Res., 112: p 5-25.

Polat, A., Kerrich, R., 2002. Nd-isotope systematics of ~2.7 Ga adakites, magnesian andesites, and arc basalts, Superior Province: evidence for shallow crustal recycling at Achaean subduction zones. Earth Planetary Science Letters, 202: p 345-360.

Rajamani, V., Shivkumar, K., Hanson, G.N., Shirey, S.B., 1985. Geochemistry and petrogenesis of amphibolites, Kolar Schist Belt, South India: evidence for komatiite magma derived by low percentages of melting of the mantle. Journal of Petrology, 26: p 92-123.

Rapp, P.R., Watson, E.B., 1986. Monazite solubility and dissolution kinematics: implications for the thorium and light rare earth element chemistry of felsic magmas. Contributions to Mineralogy and Petrology, 94: p 304-316.

Rollinson, H., 1993. Using Geochemical Data: Evaluation, Presentation, Interpretation. Pearson Education Limited, 352 pp.

Rudnick, R.L., 1995. Making continental crust. Nature, 378: p 571-578.

Schnetger, B., 1994. Partial melting during the evolution of the amphibolite- to granulite-facies gneisses of the Ivrea Zone, northern Italy. Chemical Geology, 113: p 71-101.

Sighinolfi, P., Gorgoni, C., 1978. Chemical evolution of high grade metamorphic rocks-anatexis and remotion of material from granulite terrains. Chemical Geology, 22: p 157-176.

Swager, C.P., Nelson, D.R., 1997. Extensional emplacement of a high-grade granite gneiss complex into low-grade greenstones, Eastern Goldfields, Yilgarn Craton, Western Australia. Precambrian Res., 83: p 203-219.

Taylor, S.R., McLennan, S.M., 1985. The Continental Crust: Its Composition and Evolution. Blackwell, Oxford, 312 p.

Teasdale, J.P., 1997. Understanding poorly exposed terranes – the interpretive geology and tectonothermal evolution of the western Gawler Craton. Ph.D. Thesis, University of Adelaide, Australia.

Toulkeridis, t., Clauer, N., Kröner, A., Reimer, T., Todt, W., 1999. Characterization, provenance and tectonic setting of Fig Tree greywackes from the Archaean Barberton Greenstone Belt, South Africa. Sedimentary Geology, 124: p 113-129.

Vogel, D.C., Vuollo, J.I., Alapieti, T.T., James, R.S., 1998. Tectonic, stratigraphic, and geochemical comparisons between *ca.* 2500-2440 mafic igneous events in the Canadian and Fennoscanadian Shields. Precambrian Res., 92: p 89-116.

White, J.C., Urbanczyk, K.M., 2001. Origin of a silica-oversaturated quartz trachyte-rhyolite suite through combined crustal melting, magma mixing, and fractional crystallization; the Leyva Canyon Volcano, Trans-Pecos magmatic province. Texas. Journal of Volcanology and Geothermal Research. 111; p 155-182.

Whitehouse, M.J., Kalsbeek, F., Nutman, A.P., 1998. Crustal growth and crustal recycling in the Nagssugtoqidian orogen of West Greenland: Constraints from radiogenic isotope systematics and U-Pb zircon geochronology. Precambrian Res., 91: p 365-381.

Whitehouse, M.J., Kamber, B.S., Moorbath, S., 1999. Age significance of U-Th-Pb zircon data from early Archaean rocks of west Greenland-a reassessment based on combined ion-microprobe and imaging studies. Chemical Geology, 160: p 201-224.

Williams, I.S., 1998. U-Th-Pb geochronology by ion microprobe. In: McKibben, M.A., Shanks III, W.C., Ridley, W.I. (Eds.), Applications of Microanalytical Techniques to Understanding Mineralizing Processes, Reviews in Economic Geology, 7: p 1-35.

Wolf, M.B., London, D., 1995. Incongruent dissolution of REE- and Sr-rich apatite in peraluminous granitic liquids: Differential apatite, monazite, and xenotime solubilities during anatexis. Am. Mineral., 80(7-8): p 765-775.

Wyman, D.A., Kerrich, R., Groves, D.I., 1999. Lode Gold Deposits and Archaean Mantle Plume-Island Arc Interaction, Abitibi Subprovince Canada. The Journal of Geology, 107: p 715-725.

Xie, Q., Kerrich, R., Fan, J., 1993. HFSE/REE fractionations in three komatiite-basalt sequences, Archaean Abitibi greenstone belt: implications for multiple sources at depth. Geochim. Cosmochim. Acta, 57: p 4111-4118.

Zang, W., Davies, M., Purvis, A., Daly, S., Fanning, C.M., 2002. Depositional setting of Late Archaean greenstones and metasediments in the Harris Greenstone Domain, Central Gawler Craton, South Australia. Abstract, 16th Australian Geological Convention, Abstracts Volume 67: p 57.

Appendix 1

Metamorphic relationships

Zircon overgrowths from the Kenella Gneiss yielded metamorphic age relationships with ages ranging through *ca.* 2500 to 2420 Ma (Table 1, 2; Fig. 5). This age range represents the peak regional granulite facies metamorphism of the Sleafordian Orogeny and is consistent with existing zircon U/Pb data relating to the Sleafordian Orogeny across the Gawler Craton (Daly and Fanning, 1993; Fanning, 1997, Daly *et al*., 1998). The metamorphic grade of the LHGB has been identified as lower to middle amphibolite facies (Daly and Fanning, 1993; Fanning, 1997; Zang *et al*., 2002), however two near concordant zircons 28.1 and 59.1 in the LHGB metasedimentary rock yield ages of 2493±28 Ma and 2493±22 Ma respectively. Similarly, from LHGB volcaniclastic, zircons 12.1 and 18.1 (Fig. 10) yielded ages of 2473±25 and 2524±7 Ma respectively, suggesting that the LHGB partially records effects of the Sleafordian Orogeny.

Retrogression during the Kimban Orogeny is recorded in mineral assemblages of the Kenella Gneiss (Daly and Fanning, 1993), however the duration and degree of metamorphism is not well known. Prograde metamorphic effects of the *ca*.1730 Ma Kimban Orogeny are better constrained in the southern Gawler Craton (Daly *et al*., 1998). Two near concordant analyses from Kenella Gneiss sample 494305 provided U-Pb ages of 1747±24 and 1729±10 Ma, convincing of granulite-grade Kimban metamorphism in the central Gawler Craton.

High pressure and temperature metamorphism at *ca*. 1720-1730 Ma has been identified in rocks of the Nimrod Group in the Transantarctic Mountains, Antarctica (Goodge *et al*., 2001). This high grade metamorphism at *ca*. 1720-1730 Ma is recorded in zircon overgrowths which have core ages ranging between *ca*. 3000-3100 Ma for euhedral zircons which display internal igneous growth zoning and *ca*. 2900-3000 Ma for slightly younger sector-zoned overgrowth indicative of subsequent igneous of metamorphic growth (Goodge *et al*., 2001). The documentation of widespread tectonism at ca. 1730 Ma across the entire extent of the Gawler Craton and its rifted correlatives in Antarctica (e.g. Oliver and Fanning, 1997) suggests that the Kimban Orogeny forms part of a plate-scale convergent orogenic belt.

Appendix 2

Sample lithologies and locations

Core Samples

				Interval	
Sample	Lithology	Area	Drillhole	From	To
506598	Christie Gneiss	Mt Christie	CD1	306'8"	307'8"
506600	Christie Gneiss	Mt Christie	CD1	322'5"	323'5"
506603	Christie Gneiss	Mt Christie	CD2	348'	349'
506606	Christie Gneiss	Mt Christie	CD2	371'5"	373'
506608	Kenella Gneiss	Kenella Rocks	DDH 1A	208'	210'
506613	Kenella Gneiss	Kenella Rocks	DDH 9A	222'	223'
506614	Kenella Gneiss	Kenella Rocks	DDH 9A	291'	292'
494305	Kenella Gneiss	Kenella Rocks	DDH 1A	373'	377'
494306	Kenella Gneiss	Kenella Rocks	DDH 9A	363'	364'9"
506635	LHGB metasediment	Mullina Well	TAR 85	66.6m	66.8m
495628	LHGB metasediment	Mullina Well	TAR 85	67m	71.5m
495643	LHGB volcaniclastic	Mullina Well	TAR 92	196.8m	197.7m

Field Samples

			WGS 84	
Sample	Lithology	Area	Easting	Northing
505724	Glenloth Granite	Glenloth Goldfield	511288	6560646
505725	Glenloth Granite	Glenloth Goldfield	512525	6558109
505726	Kenella Gneiss	South Lake	496872	6582033
505727	Kenella Gneiss	South Lake	497076	6582885
505728	Kenella Gneiss	South Lake	497076	6582885
505729	Christie Gneiss	Christie Corner	356888	6644871
505730	Christie Gneiss	Christie Corner	356888	6644867
505731	Christie Gneiss	Christie Corner	356886	6644868
505732	Christie Gneiss	Christie Corner	356886	6644868

Table 1
SHRIMP zircon U-Pb isotopic data for Kenella Gneiss sample 494305

							Radiogenic Ratios							Age (Ma)				
Grain. spot	U (ppm)	Th (ppm)	Th/U	^{206}Pb* (ppm)	^{204}Pb/ ^{206}Pb	f206 %	^{206}Pb/ ^{238}U	±	^{207}Pb/ ^{235}U	±	^{207}Pb/ ^{206}Pb	±	r	^{206}Pb/ ^{238}U	±	^{207}Pb/ ^{206}Pb	±	% Disc
1.1	409	173	0.42	170	0.000031	0.04	0.4834	0.0062	11.267	0.157	0.1690	0.0009	0.922	2542	27	**2548**	**9**	0
2.1	235	96	0.41	101	0.000057	0.08	0.4990	0.0071	11.807	0.235	0.1716	0.0024	0.712	2610	30	**2573**	**23**	-1
3.1	118	76	0.65	57	0.000248	0.33	0.5631	0.0101	15.293	0.367	0.1970	0.0031	0.751	2879	42	**2801**	**26**	-3
4.1	313	171	0.55	116	-	<0.01	0.4317	0.0058	9.988	0.148	0.1678	0.0010	0.908	2313	26	**2536**	**10**	10
5.1	144	48	0.33	56	0.000005	0.01	0.4541	0.0077	10.584	0.341	0.1690	0.0046	0.525	2414	34	**2548**	**46**	6
7.1	132	68	0.52	67	0.000087	0.11	0.5891	0.0101	17.817	0.373	0.2194	0.0027	0.816	2986	41	**2976**	**19**	0
8.1	241	115	0.48	108	0.000077	0.11	0.5224	0.0072	12.896	0.200	0.1790	0.0013	0.890	2709	31	**2644**	**12**	-2
9.1	591	410	0.69	252	0.000043	0.06	0.4952	0.0061	11.335	0.163	0.1660	0.0012	0.853	2593	26	**2518**	**13**	-3
10.1	478	166	0.35	197	-	<0.01	0.4794	0.0063	11.206	0.164	0.1695	0.0011	0.899	2525	28	**2553**	**11**	1
11.1	449	104	0.23	207	0.000006	0.01	0.5378	0.0086	13.715	0.228	0.1850	0.0008	0.965	2774	36	**2698**	**7**	-3
12.1	510	94	0.18	206	0.000028	0.04	0.4693	0.0057	10.155	0.158	0.1569	0.0015	0.780	2481	25	**2423**	**17**	-2
12.2	670	575	0.86	276	0.000065	0.09	0.4783	0.0117	11.224	0.278	0.1702	0.0008	0.984	2520	51	**2560**	**7**	2
13.1	1366	1749	1.28	592	0.000014	0.02	0.5044	0.0058	11.871	0.140	0.1707	0.0005	0.973	2633	25	**2564**	**5**	-3
13.2	753	30	0.04	306	0.000030	0.04	0.4725	0.0058	10.772	0.138	0.1653	0.0006	0.959	2495	25	**2511**	**6**	1
14.1	175	135	0.77	66	-	<0.01	0.4393	0.0062	9.623	0.155	0.1589	0.0012	0.875	2347	28	**2444**	**13**	4
15.1	829	592	0.71	384	0.000003	<0.01	0.5396	0.0067	15.078	0.723	0.2027	0.0094	0.257	2782	28	**2848**	**75**	2
15.2	754	115	0.15	311	0.000010	0.01	0.4799	0.0056	10.600	0.131	0.1602	0.0006	0.953	2527	25	**2458**	**6**	-3
16.1	273	244	0.89	109	0.001030	1.37	0.4607	0.0061	12.868	0.235	0.2026	0.0026	0.721	2443	27	2847	21	17
16.2	662	66	0.10	171	0.000345	0.50	0.2989	0.0036	6.190	0.089	0.1502	0.0012	0.840	1686	18	2348	13	39
17.1	164	61	0.37	69	0.000076	0.10	0.4852	0.0068	12.049	0.195	0.1801	0.0015	0.864	2550	29	**2654**	**14**	4
18.1	1744	17	0.01	685	0.000009	0.01	0.4569	0.0052	9.691	0.124	0.1538	0.0009	0.897	2426	23	**2389**	**10**	-2
19.1	133	87	0.66	59	0.000512	0.72	0.5127	0.0088	11.629	0.411	0.1645	0.0051	0.487	2668	38	**2503**	**52**	-6
20.1	374	192	0.51	161	0.000006	0.01	0.4997	0.0063	11.988	0.163	0.1740	0.0009	0.927	2612	27	**2596**	**8**	-1
21.1	141	78	0.56	63	0.000011	0.01	0.5246	0.0076	12.704	0.218	0.1756	0.0016	0.848	2719	32	**2612**	**15**	-4
22.1	685	251	0.37	286	0.000002	<0.01	0.4866	0.0058	11.252	0.139	0.1677	0.0006	0.956	2556	25	**2535**	**6**	-1
23.1	189	140	0.74	89	0.000194	0.27	0.5463	0.0076	13.411	0.225	0.1780	0.0017	0.833	2810	32	**2635**	**15**	-6
24.1	204	48	0.23	53	0.000098	0.15	0.3026	0.0059	4.460	0.106	0.1069	0.0014	0.829	1704	29	**1747**	**24**	3
25.1	221	155	0.70	101	-	<0.01	0.5310	0.0097	12.898	0.250	0.1762	0.0011	0.946	2746	41	**2617**	**10**	-5
26.1	413	407	0.99	167	0.000027	0.04	0.4695	0.0062	11.121	0.157	0.1718	0.0009	0.930	2481	27	**2575**	**9**	4
27.1	378	55	0.15	169	0.000005	0.01	0.5203	0.0069	12.924	0.415	0.1801	0.0053	0.416	2701	29	**2654**	**48**	-2
28.1	54	28	0.52	27	0.000105	0.14	0.5769	0.0125	15.108	0.382	0.1899	0.0025	0.857	2936	51	**2742**	**21**	-7
29.1	512	75	0.15	167	-	<0.01	0.3796	0.0061	8.110	0.137	0.1550	0.0007	0.959	2074	29	2401	8	16
29.2	868	657	0.76	408	0.000021	0.03	0.5464	0.0064	16.589	0.202	0.2202	0.0007	0.966	2810	27	**2982**	**5**	6
30.1	941	22	0.02	238	0.000014	0.02	0.2943	0.0035	4.294	0.057	0.1058	0.0006	0.909	1663	18	**1729**	**10**	4
31.1	47	26	0.55	19	0.000321	0.45	0.4797	0.0099	10.743	0.316	0.1624	0.0034	0.704	2526	43	**2481**	**35**	-2
32.1	631	563	0.89	263	-	<0.01	0.4857	0.0059	11.270	0.143	0.1683	0.0007	0.949	2552	25	**2541**	**7**	0
33.1	310	264	0.85	130	0.000040	0.05	0.4898	0.0063	12.169	0.170	0.1802	0.0010	0.922	2570	27	**2655**	**9**	3
34.1	131	136	1.04	56	-	<0.01	0.5033	0.0083	12.061	0.224	0.1738	0.0015	0.890	2628	36	**2595**	**14**	-1
35.1	124	58	0.47	46	0.000171	0.24	0.4292	0.0066	9.322	0.285	0.1575	0.0042	0.504	2302	30	**2429**	**45**	6
36.1	502	145	0.29	300	0.000021	0.02	0.6966	0.0089	30.115	0.397	0.3135	0.0010	0.971	3408	34	**3538**	**5**	4
37.1	388	234	0.60	147	0.000014	0.02	0.4413	0.0056	9.551	0.130	0.1570	0.0008	0.923	2356	25	**2423**	**9**	3
38.1	958	262	0.27	324	0.000075	0.11	0.3940	0.0047	8.737	0.110	0.1608	0.0007	0.943	2141	22	2464	7	15
39.1	153	44	0.29	64	0.000072	0.10	0.4889	0.0078	10.840	0.198	0.1608	0.0014	0.875	2566	34	**2464**	**15**	-4
40.1	366	198	0.54	163	0.000086	0.12	0.5188	0.0067	12.802	0.185	0.1790	0.0012	0.889	2694	28	**2643**	**11**	-2
41.1	1225	230	0.19	521	-	<0.01	0.4950	0.0058	11.942	0.177	0.1750	0.0016	0.789	2592	25	**2606**	**15**	1
42.1	445	373	0.84	191	0.000038	0.05	0.5001	0.0063	12.043	0.161	0.1747	0.0008	0.936	2614	27	**2603**	**8**	0
43.1	1130	1396	1.24	466	0.000023	0.03	0.4799	0.0057	11.159	0.138	0.1686	0.0006	0.956	2527	25	**2544**	**6**	1
43.2	505	191	0.38	213	0.000039	0.05	0.4894	0.0060	11.325	0.150	0.1678	0.0008	0.934	2568	26	**2536**	**8**	-1

Notes :
1. Uncertainties given at the one s level.
2. f206 % denotes the percentage of 206Pb that is common Pb.
3. Correction for common Pb made using the measured 204Pb/206Pb ratio.
4. For % Disc., 0% denotes a concordant analysis.

Table 2
SHRIMP zircon U-Pb isotopic data for Kenella Gneiss sample 494306

							Radiogenic Ratios							Age (Ma)				
Grain. spot	U (ppm)	Th (ppm)	Th/U	$^{206}Pb^*$ (ppm)	$^{204}Pb/^{206}Pb$	f206 %	$^{206}Pb/^{238}U$	±	$^{207}Pb/^{235}U$	±	$^{207}Pb/^{206}Pb$	±	r	$^{206}Pb/^{238}U$	±	$^{207}Pb/^{206}Pb$	±	% Disc
6.1	549	643	1.17	226	0.000023	0.03	0.4800	0.0060	11.285	0.150	0.1705	0.0008	0.933	2527	26	**2563**	**8**	1
1.1	228	172	0.76	106	0.000039	0.05	0.5419	0.0074	14.207	0.265	0.1902	0.0024	0.731	2791	31	**2744**	**21**	-2
2.1	137	142	1.04	60	0.000025	0.03	0.5117	0.0077	12.795	0.236	0.1814	0.0019	0.814	2664	33	**2665**	**18**	0
3.1	146	105	0.72	62	-	<0.01	0.4959	0.0099	12.649	0.275	0.1850	0.0016	0.915	2596	42	**2698**	**14**	4
~~4.1~~	~~160~~	~~67~~	~~0.42~~	~~112~~	~~0.000231~~	~~0.29~~	~~0.8113~~	~~0.0120~~	~~27.864~~	~~0.448~~	~~0.2491~~	~~0.0016~~	~~0.916~~	~~3830~~	~~43~~	~~3179~~	~~10~~	~~-17~~
~~5.1~~	~~151~~	~~122~~	~~0.81~~	~~64~~	~~–~~	~~<0.01~~	~~0.4975~~	~~0.0092~~	~~14.622~~	~~1.356~~	~~0.2132~~	~~0.0194~~	~~0.200~~	~~2603~~	~~40~~	~~2930~~	~~147~~	~~13~~
6.1	275	33	0.12	101	0.000077	0.11	0.4267	0.0060	9.409	0.152	0.1599	0.0013	0.873	2291	27	**2455**	**13**	7
7.1	282	141	0.50	106	0.000033	0.05	0.4369	0.0057	9.459	0.137	0.1570	0.0010	0.900	2337	25	**2424**	**11**	4
8.1	578	440	0.76	233	0.000029	0.04	0.4687	0.0056	11.127	0.141	0.1722	0.0007	0.947	2478	25	**2579**	**7**	4
9.1	188	167	0.89	81	0.000089	0.12	0.5007	0.0069	12.586	0.198	0.1823	0.0014	0.882	2617	30	**2674**	**12**	2
10.1	91	87	0.96	38	0.000015	0.02	0.4924	0.0079	11.960	0.223	0.1762	0.0017	0.863	2581	34	**2617**	**16**	1
11.1	227	176	0.77	111	-	<0.01	0.5701	0.0076	15.937	0.266	0.2028	0.0021	0.795	2908	31	**2849**	**16**	-2
12.1	55	33	0.60	25	-	<0.01	0.5325	0.0097	14.354	0.321	0.1955	0.0025	0.819	2752	41	**2789**	**21**	1
13.1	292	37	0.13	126	-	<0.01	0.5001	0.0068	11.247	0.165	0.1631	0.0009	0.926	2614	29	**2488**	**9**	-5
14.1	116	215	1.85	58	-	<0.01	0.5757	0.0086	14.371	0.240	0.1811	0.0013	0.898	2931	35	**2663**	**12**	-9
15.1	381	43	0.11	157	-	<0.01	0.4814	0.0062	12.760	0.175	0.1923	0.0009	0.944	2533	27	**2762**	**7**	9
16.1	390	19	0.05	164	0.000047	0.07	0.4884	0.0069	10.715	0.160	0.1591	0.0008	0.945	2564	30	**2446**	**8**	-5
17.1	649	31	0.05	237	0.000010	0.01	0.4240	0.0051	8.971	0.132	0.1535	0.0013	0.826	2278	23	**2385**	**14**	5
18.1	573	182	0.32	230	0.000026	0.04	0.4671	0.0055	10.427	0.135	0.1619	0.0009	0.904	2471	24	**2476**	**9**	0
19.1	212	50	0.24	86	0.001444	2.03	0.4614	0.0068	10.556	0.267	0.1659	0.0034	0.582	2446	30	**2517**	**35**	3
20.1	115	29	0.26	44	-	<0.01	0.4484	0.0071	9.661	0.174	0.1562	0.0014	0.876	2388	31	**2415**	**15**	1
21.1	147	38	0.26	52	0.000110	0.16	0.4088	0.0058	8.785	0.158	0.1559	0.0017	0.792	2209	27	**2411**	**19**	9
22.1	207	97	0.47	97	0.000063	0.09	0.5443	0.0069	13.842	0.193	0.1844	0.0010	0.915	2802	29	**2693**	**9**	-4
23.1	82	67	0.81	41	-	<0.01	0.5841	0.0091	17.809	0.333	0.2211	0.0023	0.836	2965	37	**2989**	**17**	1
24.1	380	161	0.42	163	-	<0.01	0.5009	0.0060	12.469	0.178	0.1805	0.0014	0.845	2618	26	**2658**	**13**	2
25.1	467	35	0.07	191	0.000032	0.04	0.4761	0.0057	10.525	0.134	0.1603	0.0007	0.938	2510	25	**2459**	**7**	-2
26.1	102	83	0.82	45	0.000048	0.07	0.5103	0.0075	12.396	0.211	0.1762	0.0015	0.866	2658	32	**2617**	**14**	-2
27.1	410	49	0.12	157	-	<0.01	0.4463	0.0056	9.358	0.124	0.1521	0.0007	0.942	2379	25	**2370**	**8**	0
28.1	395	35	0.09	156	0.000003	0.00	0.4593	0.0062	10.239	0.146	0.1617	0.0007	0.951	2437	28	**2473**	**7**	1
29.1	198	111	0.56	87	-	<0.01	0.5085	0.0066	11.877	0.173	0.1694	0.0011	0.898	2650	28	**2552**	**11**	-4
30.1	241	158	0.66	108	-	<0.01	0.5200	0.0065	12.776	0.171	0.1782	0.0009	0.929	2699	28	**2636**	**8**	-2
31.1	76	40	0.53	30	0.000029	0.04	0.4527	0.0079	10.156	0.221	0.1627	0.0021	0.798	2407	35	**2484**	**22**	3
32.1	168	49	0.29	75	0.000020	0.03	0.5225	0.0069	13.228	0.192	0.1836	0.0011	0.909	2710	29	**2686**	**10**	-1
33.1	598	85	0.14	230	0.000019	0.03	0.4477	0.0051	9.682	0.136	0.1569	0.0013	0.817	2385	23	**2422**	**14**	2
34.1	323	109	0.34	142	0.000071	0.10	0.5097	0.0064	12.245	0.165	0.1742	0.0008	0.934	2655	27	**2599**	**8**	-2
35.1	80	71	0.88	38	-	<0.01	0.5482	0.0082	14.498	0.251	0.1918	0.0017	0.866	2818	34	**2758**	**14**	-2
36.1	121	150	1.24	57	0.000034	0.05	0.5479	0.0081	13.721	0.225	0.1816	0.0013	0.902	2816	34	**2668**	**12**	-5
37.1	548	41	0.07	213	-	<0.01	0.4526	0.0051	9.676	0.116	0.1551	0.0006	0.951	2407	23	**2402**	**6**	0
38.1	139	138	1.00	63	0.000158	0.22	0.5246	0.0074	12.989	0.338	0.1796	0.0039	0.545	2719	31	**2649**	**36**	-3
39.1	303	195	0.64	127	0.000006	0.01	0.4864	0.0058	11.496	0.146	0.1714	0.0008	0.935	2555	25	**2572**	**8**	1
40.1	119	68	0.57	57	0.000062	0.08	0.5532	0.0075	14.637	0.271	0.1919	0.0024	0.729	2838	31	**2758**	**21**	-3
41.1	204	122	0.60	87	-	<0.01	0.4968	0.0061	11.905	0.160	0.1738	0.0009	0.915	2600	26	**2594**	**9**	0
42.1	109	57	0.53	52	0.000002	<0.01	0.5599	0.0078	14.444	0.227	0.1871	0.0013	0.892	2866	32	**2717**	**12**	-5
~~43.1~~	~~106~~	~~56~~	~~0.53~~	~~81~~	~~0.023595~~	~~31.89~~	~~0.6040~~	~~0.0237~~	~~16.525~~	~~4.772~~	~~0.1984~~	~~0.0568~~	~~0.136~~	~~3046~~	~~95~~	~~2813~~	~~468~~	~~-8~~
44.1	615	27	0.04	216	-	<0.01	0.4093	0.0046	8.388	0.100	0.1486	0.0006	0.948	2212	21	**2330**	**7**	5
45.1	197	164	0.83	90	0.000047	0.06	0.5333	0.0069	13.428	0.236	0.1826	0.0022	0.740	2755	29	**2677**	**20**	-3
46.1	114	120	1.05	53	0.000026	0.04	0.5358	0.0084	13.617	0.239	0.1843	0.0015	0.891	2766	35	**2692**	**13**	-3
47.1	236	267	1.13	110	-	<0.01	0.5447	0.0067	14.999	0.198	0.1997	0.0009	0.933	2803	28	**2824**	**8**	1
48.1	567	369	0.65	345	0.000009	0.01	0.7088	0.0083	28.608	0.342	0.2927	0.0007	0.979	3454	31	**3432**	**4**	-1
49.1	394	200	0.51	138	0.000010	0.02	0.4082	0.0053	8.061	0.112	0.1432	0.0008	0.922	2207	24	**2266**	**9**	3
50.1	418	58	0.14	168	0.000059	0.08	0.4668	0.0056	10.134	0.174	0.1574	0.0019	0.700	2470	25	**2428**	**21**	-2
51.1	54	40	0.74	24	0.000411	0.57	0.5219	0.0097	12.384	0.325	0.1721	0.0032	0.709	2707	41	**2578**	**31**	-5
~~52.1~~	~~104~~	~~40~~	~~0.38~~	~~63~~	~~0.000537~~	~~0.70~~	~~0.7032~~	~~0.0181~~	~~21.326~~	~~0.584~~	~~0.2199~~	~~0.0020~~	~~0.942~~	~~3433~~	~~69~~	~~2980~~	~~15~~	~~-13~~
53.1	132	70	0.53	58	0.000030	0.04	0.5110	0.0116	13.117	0.314	0.1862	0.0014	0.952	2661	50	**2709**	**12**	2

Notes : Refer to Table 1.

Table 3
SHRIMP zircon U-Pb isotopic data for LHGB metasedimentary rock sample 495628

							Radiogenic Ratios							Age (Ma)				
Grain. spot	U (ppm)	Th (ppm)	Th/U	^{206}Pb* (ppm)	^{204}Pb/ ^{206}Pb	f206 %	^{206}Pb/ ^{238}U	±	^{207}Pb/ ^{235}U	±	^{207}Pb/ ^{206}Pb	±	r	^{206}Pb/ ^{238}U	±	^{207}Pb/ ^{206}Pb	±	% Disc
1.1	125	54	0.43	48	0.000149	0.21	.44982	.00779	10.464	0.225	0.1687	0.0022	0.804	2394	35	**2545**	**21**	6
2.1	142	93	0.66	56	0.003123	4.40	.44333	.00821	10.066	0.810	0.1647	0.0129	0.230	2366	37	**2504**	**132**	6
3.1	181	122	0.67	73	0.000080	0.11	.46682	.00680	10.874	0.183	0.1689	0.0014	0.865	2470	30	**2547**	**14**	3
4.1	142	135	0.95	57	0.000000	0.00	.46426	.00759	10.717	0.222	0.1674	0.0021	0.789	2458	33	**2532**	**21**	3
5.1	325	210	0.65	120	0.002907	4.06	.41299	.00587	9.736	0.356	0.1710	0.0058	0.388	2229	27	2567	56	15
6.1	207	169	0.82	76	0.002260	3.14	.41334	.00656	9.837	0.328	0.1726	0.0051	0.476	2230	30	2583	49	16
7.1	208	193	0.93	64	0.001602	2.16	.34776	.00549	9.284	0.290	0.1936	0.0052	0.506	1924	26	2773	44	44
8.1	160	144	0.90	65	0.007597	10.38	.42354	.00820	10.824	0.929	0.1853	0.0155	0.226	2277	37	2701	138	19
9.1	266	336	1.26	73	0.002514	3.45	.30956	.00468	7.778	0.264	0.1822	0.0055	0.446	1739	23	2673	50	54
10.1	216	294	1.36	82	0.001908	2.66	.43115	.00685	10.237	0.337	0.1722	0.0050	0.482	2311	31	2579	48	12
11.1	253	112	0.44	104	0.000058	0.08	.48044	.00753	11.072	0.193	0.1671	0.0013	0.901	2529	33	**2529**	**13**	0
12.1	190	127	0.67	68	0.000832	1.16	.40901	.00632	9.732	0.220	0.1726	0.0028	0.685	2210	29	2583	27	17
13.1	176	69	0.39	45	0.000994	1.36	.29003	.00477	7.289	0.183	0.1823	0.0035	0.654	1642	24	2674	31	63
14.1	176	154	0.88	60	0.003306	4.63	.38195	.00660	8.865	0.458	0.1683	0.0082	0.334	2085	31	2541	82	22
15.1	194	135	0.69	75	0.000890	1.24	.44393	.00756	10.415	0.260	0.1702	0.0031	0.681	2368	34	**2559**	**31**	8
16.1	290	342	1.18	73	0.007095	9.75	.26402	.00492	6.612	0.536	0.1816	0.0143	0.230	1510	25	2668	131	77
17.1	231	171	0.74	94	0.000567	0.80	.46938	.00737	10.780	0.221	0.1666	0.0022	0.766	2481	32	**2524**	**22**	2
18.1	152	69	0.45	60	0.000421	0.59	.45500	.00807	10.407	0.251	0.1659	0.0027	0.734	2417	36	**2517**	**28**	4
19.1	235	214	0.91	95	0.001524	2.14	.46018	.00744	10.654	0.303	0.1679	0.0039	0.568	2440	33	**2537**	**39**	4
20.1	207	117	0.56	79	0.000874	1.22	.43932	.00743	10.143	0.253	0.1675	0.0031	0.679	2348	33	**2532**	**31**	8
21.1	247	296	1.20	100	0.002163	2.99	.45790	.00846	11.159	0.389	0.1768	0.0052	0.530	2430	37	**2623**	**49**	8
22.1	176	261	1.48	69	0.000990	1.37	.44630	.01280	10.837	0.395	0.1761	0.0039	0.788	2379	57	**2617**	**37**	10
23.1	152	86	0.57	62	0.000492	0.69	.47093	.00811	10.614	0.248	0.1635	0.0026	0.737	2488	36	**2492**	**27**	0
23.2	215	121	0.56	77	0.001541	2.16	.40515	.00651	9.332	0.268	0.1670	0.0040	0.559	2193	30	2528	40	15
24.1	196	292	1.49	72	0.003784	5.33	.40432	.00687	9.201	0.520	0.1651	0.0089	0.301	2189	32	2508	91	15
25.1	225	154	0.68	82	0.001088	1.49	.41957	.00637	10.425	0.237	0.1802	0.0030	0.668	2259	29	2655	28	18
26.1	374	286	0.77	132	0.000927	1.30	.40606	.00552	9.468	0.186	0.1691	0.0024	0.691	2197	25	2549	24	16
27.1	226	118	0.52	89	0.000096	0.13	.45775	.00677	10.743	0.182	0.1702	0.0014	0.874	2430	30	**2560**	**14**	5
28.1	144	60	0.42	58	0.000658	0.93	.46640	.00767	10.520	0.247	0.1636	0.0027	0.700	2468	34	**2493**	**28**	1
29.1	174	110	0.64	68	0.001145	1.59	.44757	.00716	10.579	0.264	0.1714	0.0033	0.639	2384	32	**2572**	**32**	8
30.1	144	176	1.22	56	0.002167	3.05	.43971	.00833	10.021	0.380	0.1653	0.0054	0.499	2349	37	**2510**	**55**	7
31.1	162	133	0.82	62	0.002851	3.93	.42585	.00753	10.437	0.422	0.1778	0.0065	0.437	2287	34	2632	61	15
32.1	115	70	0.61	42	0.000138	0.19	.42699	.00765	9.965	0.227	0.1693	0.0024	0.786	2292	35	2550	24	11
~~33.1~~	~~593~~	~~595~~	~~1.00~~	~~68~~	~~0.009607~~	~~12.48~~	~~.11590~~	~~.00227~~	~~3.545~~	~~0.305~~	~~0.2218~~	~~0.0186~~	~~0.228~~	~~707~~	~~13~~	~~2994~~	~~135~~	~~324~~
34.1	189	94	0.50	71	0.000995	1.37	.42864	.00683	10.640	0.255	0.1800	0.0032	0.665	2300	31	2653	30	15
35.1	130	78	0.60	52	-	<0.01	.46913	.00920	10.761	0.241	0.1664	0.0018	0.875	2480	40	**2521**	**18**	2
36.1	152	120	0.79	62	0.000850	1.18	.46874	.00816	11.355	0.300	0.1757	0.0035	0.658	2478	36	**2613**	**33**	5
37.1	136	100	0.74	52	0.000103	0.14	.44391	.00854	10.528	0.234	0.1720	0.0019	0.866	2368	38	**2577**	**19**	9
38.1	143	76	0.54	58	0.000161	0.23	.46890	.00830	10.777	0.232	0.1667	0.0020	0.823	2479	36	**2525**	**20**	2
39.1	97	50	0.51	36	0.000561	0.79	.42539	.00807	9.541	0.265	0.1627	0.0033	0.683	2285	36	**2483**	**34**	9
40.1	223	139	0.63	80	0.000422	0.59	.41452	.00672	9.704	0.202	0.1698	0.0022	0.779	2236	31	2555	22	14
41.1	350	161	0.46	102	0.003689	5.13	.32160	.00491	7.657	0.352	0.1727	0.0075	0.332	1798	24	2584	72	44
42.1	268	131	0.49	104	0.000273	0.38	.45126	.00679	10.431	0.186	0.1676	0.0016	0.844	2401	30	**2534**	**16**	6
43.1	166	143	0.86	61	0.002574	3.50	.41199	.00717	10.657	0.673	0.1876	0.0114	0.276	2224	33	2721	100	22
44.1	175	125	0.72	70	0.001226	1.69	.45471	.00756	11.132	0.277	0.1776	0.0033	0.668	2416	33	**2630**	**31**	9
45.1	198	82	0.41	75	0.000458	0.64	.43503	.00632	9.995	0.196	0.1666	0.0022	0.742	2328	28	**2524**	**22**	8
~~46.1~~	~~477~~	~~1920~~	~~4.03~~	~~61~~	~~0.010683~~	~~14.61~~	~~.12618~~	~~.00286~~	~~3.234~~	~~0.421~~	~~0.1859~~	~~0.0238~~	~~0.174~~	~~766~~	~~16~~	~~2706~~	~~212~~	~~253~~
47.1	204	183	0.90	77	0.000443	0.62	.43554	.00681	10.064	0.201	0.1676	0.0021	0.783	2331	31	**2534**	**21**	9
48.1	188	63	0.33	74	0.000294	0.41	.45528	.00674	10.424	0.196	0.1661	0.0019	0.786	2419	30	**2518**	**20**	4
49.1	532	748	1.41	192	0.003450	4.69	.39996	.00559	10.357	0.396	0.1878	0.0067	0.365	2169	26	2723	59	26
50.1	212	121	0.57	77	0.001369	1.90	.41572	.00728	9.886	0.269	0.1725	0.0036	0.644	2241	33	2582	35	15
~~51.1~~	~~299~~	~~995~~	~~3.33~~	~~99~~	~~0.020242~~	~~22.57~~	~~.29892~~	~~.01226~~	~~16.704~~	~~1.871~~	~~0.4053~~	~~0.0422~~	~~0.366~~	~~1686~~	~~61~~	~~3929~~	~~157~~	~~133~~
52.1	169	88	0.52	66	0.000170	0.24	.45199	.01038	10.483	0.265	0.1682	0.0018	0.908	2404	46	**2540**	**18**	6
53.1	420	352	0.84	147	0.000863	1.21	.40281	.00513	9.395	0.171	0.1692	0.0022	0.700	2182	24	2549	22	17
54.1	110	51	0.47	44	0.001580	2.21	.45470	.00826	10.523	0.336	0.1678	0.0044	0.569	2416	37	**2536**	**44**	5
55.1	216	200	0.93	85	0.002936	3.90	.44137	.00641	12.442	0.404	0.2045	0.0059	0.447	2357	29	2862	47	21
56.1	320	767	2.39	75	0.003772	5.15	.25760	.00390	6.586	0.322	0.1854	0.0086	0.310	1478	20	2702	77	83
57.1	194	116	0.60	77	0.000201	0.28	.46129	.00650	10.487	0.176	0.1649	0.0015	0.839	2445	29	**2506**	**15**	2
58.1	269	206	0.76	110	0.000069	0.10	.47470	.00627	10.869	0.160	0.1661	0.0011	0.896	2504	27	**2518**	**11**	1
59.1	85	35	0.41	34	0.000241	0.34	.46525	.00893	10.496	0.244	0.1636	0.0021	0.826	2463	39	**2493**	**22**	1

Notes : Refer to Table 1.

Table 4
SHRIMP zircon U-Pb isotopic data for LHGB volcaniclastic rock sample 495643

							Radiogenic Ratios							Age (Ma)				
Grain. spot	U (ppm)	Th (ppm)	Th/U	^{206}Pb* (ppm)	^{204}Pb/ ^{206}Pb	f206 %	^{206}Pb/ ^{238}U	±	^{207}Pb/ ^{235}U	±	^{207}Pb/ ^{206}Pb	±	r	^{206}Pb/ ^{238}U	±	^{207}Pb/ ^{206}Pb	±	% Disc
1.1	138	57	0.41	55	0.000052	0.07	0.4652	0.0065	10.634	0.168	0.1658	0.0012	0.885	2462	29	**2516**	**12**	2
2.1	103	35	0.34	44	0.000034	0.05	0.4956	0.0074	11.446	0.194	0.1675	0.0013	0.880	2595	32	**2533**	**13**	-2
3.1	374	176	0.47	126	0.000052	0.07	0.3907	0.0046	8.690	0.110	0.1613	0.0008	0.925	2126	21	2470	8	16
4.1	103	33	0.32	43	0.000016	0.02	0.4823	0.0072	11.168	0.192	0.1679	0.0014	0.865	2537	31	**2537**	**14**	0
5.1	137	72	0.53	56	0.000182	0.26	0.4753	0.0067	10.849	0.179	0.1655	0.0014	0.851	2507	29	**2513**	**15**	0
6.1	73	24	0.34	31	0.000166	0.23	0.4889	0.0144	11.152	0.350	0.1654	0.0018	0.937	2566	62	**2512**	**18**	-2
7.1	350	343	0.98	142	0.000056	0.08	0.4708	0.0058	10.734	0.142	0.1653	0.0008	0.938	2487	26	**2511**	**8**	1
8.1	603	297	0.49	188	0.000297	0.42	0.3613	0.0058	8.076	0.151	0.1621	0.0015	0.863	1988	28	2478	16	25
9.1	116	54	0.47	50	0.000000	0.00	0.5007	0.0080	11.613	0.206	0.1682	0.0013	0.904	2617	35	**2540**	**13**	-3
10.1	203	121	0.59	83	0.000049	0.07	0.4748	0.0062	10.940	0.157	0.1671	0.0010	0.906	2505	27	**2529**	**10**	1
11.1	99	33	0.33	39	0.000080	0.11	0.4634	0.0065	10.715	0.170	0.1677	0.0013	0.879	2455	28	**2535**	**13**	3
12.1	44	14	0.32	17	0.000237	0.33	0.4545	0.0080	10.128	0.231	0.1616	0.0024	0.770	2415	35	**2473**	**25**	2
13.1	214	155	0.72	87	0.000056	0.08	0.4700	0.0057	10.638	0.140	0.1642	0.0008	0.931	2484	25	**2499**	**8**	1
14.1	139	98	0.71	56	0.000141	0.20	0.4694	0.0062	10.697	0.158	0.1653	0.0011	0.892	2481	27	**2510**	**11**	1
15.1	80	32	0.40	32	0.000028	0.04	0.4703	0.0070	10.972	0.185	0.1692	0.0014	0.878	2485	31	**2550**	**14**	3
16.1	101	38	0.38	42	0.000156	0.22	0.4815	0.0068	10.932	0.178	0.1647	0.0013	0.874	2534	30	**2504**	**13**	-1
17.1	134	93	0.69	55	0.000000	0.00	0.4807	0.0064	11.021	0.163	0.1663	0.0010	0.906	2530	28	**2521**	**10**	0
18.1	393	279	0.71	147	0.000040	0.06	0.4358	0.0050	9.443	0.115	0.1572	0.0006	0.945	2332	22	**2425**	**7**	4
19.1	275	163	0.59	102	0.000000	0.00	0.4339	0.0054	9.967	0.133	0.1666	0.0008	0.935	2323	24	**2524**	**8**	9
20.1	56	20	0.36	23	0.000224	0.32	0.4701	0.0084	10.646	0.239	0.1642	0.0022	0.793	2484	37	**2500**	**23**	1

Notes : Refer to Table 1.

Table 5
Chemical composition for rocks of the Mulgathing Complex

Lithology	*Glenloth Granite*		*Lake Harris Greenstone Belt*			*Kenella Gneiss*								*Christie Gneiss*							
Sample	505724	505725	495628	506635	495643	506608	506613	506614	494305	494306	505726	505727	505728	506598	506600	506603	506606	505729	505730	505731	505732
Location	Glenloth	Goldfield	TAR 85	TAR 85	TAR 92	DDH 1A	DDH 9A	DDH 9A	DDH 1A	DDH 9A	South Lake			CD1	CD1	CD2	CD2	Christie Corner			
Major Elements (wt %)																					
SiO2	68.	72.9	63.2	49.	70.2	64.9	63.8	64.1	67.5	67.5	75.3	39.4	57.8	54.8	71.5	47.7	69.2	68.4	66.4	58.8	69.3
TiO2	0.33	0.09	0.47	0.26	0.49	0.69	0.63	0.82	0.6	0.58	0.04	1.17	0.62	4.28	0.48	1.32	0.54	0.68	0.63	0.95	0.36
Al2O3	16.7	16.1	12.4	6.94	11.9	17.5	17.	17.8	15.6	14.3	14.	33.8	16.3	15.9	12.2	18.2	15.5	15.3	16.1	18.7	14.6
Fe2O3	3.04	0.89	8.39	18.9	5.69	5.52	6.83	5.74	5.77	4.65	0.51	13.5	7.	16.	7.29	23.5	5.2	5.11	6.47	8.85	6.85
MnO	0.06	0.01	0.1	0.22	0.23	0.03	0.09	0.1	0.08	0.09	0.02	0.19	0.14	0.13	0.09	0.28	0.06	0.07	0.1	0.12	0.12
MgO	0.85	0.25	4.05	6.41	2.12	1.96	3.3	2.91	2.63	3.08	0.08	4.	3.49	6.13	2.55	5.28	2.24	2.36	2.68	4.17	2.62
CaO	3.14	3.47	2.15	6.34	3.16	0.83	2.42	1.17	0.85	2.1	0.69	1.98	11.4	0.63	1.51	1.09	1.67	2.21	2.19	1.43	1.8
Na2O	4.85	5.29	2.08	0.99	1.81	1.07	1.36	2.29	1.39	1.85	4.65	2.06	2.98	0.26	2.	0.92	2.04	2.98	3.07	2.11	2.69
K2O	2.5	0.87	1.66	0.61	2.24	3.47	2.14	2.89	3.03	2.29	3.65	3.52	0.66	1.42	1.86	2.44	3.47	2.76	2.46	3.7	1.85
P2O5	0.11	0.02	0.06	0.13	0.12	0.04	0.13	0.04	0.03	0.05	0.02	0.03	0.15	0.06	0.05	0.23	0.07	0.05	0.06	0.04	0.04
S	0.01	0.01	0.04	0.09	0.18	0.27	0.22	0.09	0.07	0.05	-	0.01	0.05	0.04	0.22	-	0.18	0.01	-	0.01	-
LOI	1.07	0.96	4.73	10.3	1.94	3.62	2.	2.4	2.91	3.24	0.82	1.5	0.86	0.64	0.47	-	0.91	0.53	0.68	1.2	0.56
Total	99.59	99.9	94.6	89.89	98.14	96.28	97.92	97.95	97.55	96.54	98.96	99.66	100.59	99.65	99.75	100.96	100.17	99.93	100.16	98.88	100.23
Trace Elements (ppm)																					
Ni	4.	-	6.5	7.	14.	3.3	6.5	3.2	6.5	10.5	-	94.	34.	25.	33.	74.	14.5	20.	55.	81.	39.
Cr	0.	0.	550.	200.	140.	50.	190.	90.	140.	130.	0.	350.	70.	120.	210.	60.	160.	160.	160.	270.	150.
Cu	6.5	17.	23.	23.	31.5	21.	46.5	28.	41.	37.	4.5	7.5	5.5	37.	340.	8.5	49.5	18.	35.	31.5	38.5
Co	43.5	49.5	42.5	24.	44.	29.	45.	34.5	40.5	45.5	53.	56.	45.	69.	65.	59.	46.	41.	50.	53.	58.
Sc	-	-	15.	5.	10.	5.	15.	10.	15.	10.	-	45.	15.	20.	20.	35.	10.	10.	15.	20.	20.
V	30.	0.	110.	40.	70.	80.	110.	110.	110.	90.	0.	290.	100.	170.	70.	80.	40.	100.	110.	180.	70.
Zn	64.	18.	74.	47.5	47.	120.	72.	69.	89.	77.	21.5	650.	73.	250.	74.	150.	65.	63.	71.	125.	72.
Ga	22.	15.	15.	8.5	15.	22.	21.	22.	21.5	19.	20.	31.5	19.	29.5	14.5	17.5	17.5	18.5	18.5	25.5	16.5
Ba	550.	165.	600.	90.	220.	550.	700.	650.	600.	420.	600.	800.	310.	210.	400.	430.	850.	650.	490.	750.	360.
Rb	89.	17.5	73.	21.5	90.	86.	72.	76.	120.	90.	49.	150.	24.	76.	57.	79.	69.	83.	76.	110.	53.
Sr	440.	450.	175.	45.	130.	85.	250.	175.	90.	145.	220.	105.	440.	20.	145.	80.	190.	340.	270.	250.	240.
Zr	150.	60.	120.	60.	120.	190.	160.	160.	150.	130.	40.	120.	120.	50.	360.	30.	220.	220.	180.	200.	280.
Y	11.	1.4	195.	88.	66.	35.	70.	54.	61.	57.	4.9	36.	17.	44.	73.	22.	52.	12.	20.	14.5	25.5
Nb	8.	1.	4.5	2.5	5.5	8.5	5.5	7.	9.	5.5	0.5	10.5	5.	64.	4.	30.5	6.	4.5	3.	6.5	3.
Th	8.5	1.75	6.	3.6	6.	6.	17.5	10.	11.	9.	0.4	17.	3.4	28.	3.6	250.	22.5	14.5	20.	13.	14.5
Pb	19.	40.5	12.	7.5	14.5	23.	28.5	22.5	94.	42.	23.5	8.5	6.5	6.	180.	15.	30.5	24.	21.5	26.5	32.5
Ta	-	-	-	-	-	-	-	-	-	-	-	-	-	-	-	-	-	-	-	-	-
U	0.66	0.4	0.8	1.	1.7	0.88	1.7	1.2	1.4	1.85	0.4	1.35	0.94	1.3	0.9	7.5	1.2	0.97	1.35	1.45	2.
Rare Earth Elements (ppm)																					
La	25.	8.5	12.5	13.5	25.	27.5	50.	33.5	35.	27.	7.	57.	24.	41.	18.	340.	46.	50.	51.	47.5	42.5
Ce	37.5	12.5	21.5	24.5	44.5	48.	93.	62.	62.	51.	10.5	98.	46.	84.	30.5	700.	86.	83.	85.	79.	67.
Pr	4.9	1.4	2.7	3.	6.	6.	11.5	7.5	7.5	6.5	1.45	12.5	6.5	11.5	3.5	93.	10.5	10.	10.5	9.	8.5
Nd	18.	4.7	9.	10.	20.	20.	40.5	27.5	25.5	23.	5.5	46.	28.5	40.5	11.5	330.	35.5	35.5	37.5	34.	30.
Sm	3.5	0.63	1.5	1.75	3.8	2.9	6.5	4.5	4.2	4.1	0.81	8.	6.	7.5	2.6	60.	6.	5.5	6.	5.5	5.5
Eu	1.	0.68	0.69	0.43	1.	1.25	1.55	1.05	1.05	1.2	0.42	1.15	1.4	0.2	0.83	1.2	1.2	1.6	1.55	1.65	1.2
Gd	3.1	0.45	1.2	1.3	3.1	1.8	3.6	2.4	2.5	2.8	0.75	6.	4.9	6.	4.	32.5	3.8	4.1	5.	4.3	5.
Tb	0.5	0.07	0.21	0.2	0.49	0.21	0.41	0.25	0.31	0.43	0.15	1.05	0.74	1.05	1.	4.1	0.6	0.6	0.8	0.6	1.
Dy	2.7	0.31	1.2	1.1	2.5	0.85	1.55	0.88	1.3	2.	0.97	7.5	4.	5.	6.	17.	2.9	3.1	4.7	3.3	6.
Ho	0.55	0.07	0.23	0.2	0.48	0.13	0.24	0.13	0.22	0.36	0.23	1.8	0.83	0.84	1.15	2.4	0.52	0.6	1.	0.73	1.25
Er	1.4	0.15	0.75	0.7	1.6	0.35	0.7	0.3	0.7	1.15	0.65	5.	2.2	2.5	3.9	6.	1.65	1.5	2.7	2.1	3.3
Tm	0.15	-	0.1	0.1	0.2	-	0.1	-	0.1	0.15	0.1	0.75	0.3	0.3	0.55	0.7	0.25	0.2	0.4	0.3	0.45
Yb	0.85	0.15	0.9	0.65	1.5	0.35	0.6	0.3	0.8	1.05	0.5	4.2	1.55	2.	3.5	3.9	1.55	1.15	2.2	1.7	2.6
Lu	0.14	0.03	0.13	0.1	0.22	0.06	0.1	0.05	0.13	0.15	0.09	0.69	0.27	0.27	0.51	0.54	0.24	0.2	0.38	0.29	0.43

Table 6
Sm-Nd isotopic data for rocks of the Mulgathing Complex

Sample	Description	Age *t* (Ma)	Sm (ppm)	Nd (ppm)	$^{147}Sm/^{144}Nd$	$^{143}Nd/^{144}Nd$[a]	$\varepsilon_{Nd}(0)$[b]	$\varepsilon_{Nd}(t)$	T_{DM}[c] (Ma)
Glenloth Granite									
505724	Granite	2500	4.091	22.11	0.1118	0.511238±8	-27.3	-0.06	2867
505725	Granite	2500	0.604	3.93	0.0928	0.510916±9	-33.6	-0.20	2818
Lake Harris Greenstone Belt									
495628	Metasedimentary rock	2505	1.500	8.86	0.1023	0.511021±22	-31.5	-1.16	2915
495643	Volcaniclastic rock	2505	3.411	19.3	0.1068	0.511085±12	-30.3	-1.36	2947
Kenella Gneiss									
494305	Metapelite	2530	3.797	23.08	0.0995	0.511011±9	-31.7	-0.12	2857
494306	Metapelite	2530	3.857	22.22	0.1049	0.511016±8	-31.6	-1.81	2992
506613	Metapelite	2530	5.988	36.98	0.0979	0.511024±9	-31.5	0.65	2801
506614	Metapelite	2530	5.263	32.03	0.0993	0.511033±9	-31.3	0.35	2825
Christie Gneiss									
506598	Metapelite	2530	8.464	43.2	0.1184	0.511165±8	-28.7	-3.31	3178
506606	Metapelite	2530	5.238	32.0	0.0989	0.510916±9	-33.6	-1.81	2968
Devil's Playground Volcanics (*data from* Cowley and Fanning, 1992)									
6037 RS27	Rhyodacite, DP1	2558	5.020	23.9	0.1273	0.51152	-22.0	0.81	2879
6037 RS31	Rhyodacite, DP1	2558	3.760	17.6	0.1287	0.51150	-22.5	-0.14	2970
6037 RS32	Rhyodacite, DP1	2558	5.640	27.0	0.1266	0.51158	-22.9	0.22	2929
6037 RS33	Rhyodacite, DP1	2558	4.920	22.9	0.1301	0.51155	-21.6	0.38	2930
6037 RS34	Rhyodacite, DP1	2558	4.950	24.1	0.1245	0.51144	-23.6	0.19	2923
6037 RS25	Andesite, DP1	2558	4.620	20.8	0.1341	0.51171	-18.3	2.37	2757
6037 RS26	Andesite, DP1	2558	3.660	17.4	0.1272	0.51161	-20.3	2.61	2720
6037 RS29	Andesite, DP1	2558	3.500	14.4	0.1467	0.51175	-17.6	-1.10	3190
6037 RS30	Andesite, DP1	2558	3.310	14.7	0.1359	0.51161	-20.3	-0.25	3019

[a] Errors on $^{143}Nd/^{144}Nd$ measurements are 2σ (mean) and refer to the last significant fugure(s).

[b] Measured ε_{Nd} values calculated with present-day CHUR $^{143}Nd/^{144}Nd$ and $^{147}Sm/^{144}Nd$ ratios of 0.512638 and 0.1966.

[c] Depleted mantle Nd model ages calculated as in Goldstein *et al* (1984).

Figure Captions

Fig. 1. Distribution of Late Archaean rocks in the Gawler Craton, South Australia.

Fig. 2. Regional aeromagnetic interpretation of simplified geology of the Mulgathing Complex, central Gawler Craton (*Modified after*: Cowley and Fanning, 1992; Daly and Fanning, 1993).

Fig. 3. Simplified geology of the Lake Harris Greenstone Belt (LHGB) domain, Mulgathing Complex, central Gawler Craton (*Modified after*: Daly and Fanning, 1993).

Fig. 4. U-Pb concordia plots showing all analytical data points for zircons from Kenella Gneiss samples (a) 494305, (b) 494306 and LHGB metasedimentary and volcaniclastic rock samples (c) 495628, (d) 495643.

Fig. 5. Combined histogram and cumulative gaussian distribution curves showing the dominant zircon $^{207}Pb/^{206}Pb$ age (Ma) populations for Kenella Gneiss samples (a) 494305, (b) 494306 and LHGB metasedimentary and volcaniclastic rock samples (c) 495628, (d) 495643. Data is filtered to exclude analyses >10% discordant and that have abundant common Pb (f206>2%).

Fig. 6. Cathodoluminescence (CL) images of selected zircons from Kenella Gneiss sample 494305. Ages in Ma.

Fig. 7. Cathodoluminescence (CL) images of selected zircons from Kenella Gneiss sample 494306. Ages in Ma.

Fig. 8. $^{207}Pb/^{206}Pb$ age (Ma) vs. Th/U ratio for zircons from Kenella Gneiss samples (a) 494305, (b) 494306 and LHGB metasedimentary and volcaniclastic rock samples (c) 495628, (d) 495643. Th/U ratios ≥ 0.2 for detrital zircons older than *ca*. 2530 Ma in the Kenella Gneiss are characteristic of an igneous provenance (e.g. Whitehouse *et al*., 1999), as opposed to Th/U ratios ≤ 0.2 which are characteristic of metamorphic zircons (e.g. Whitehouse *et al*, 1999), and are younger than *ca*. 2500 Ma. Data is filtered to exclude analyses that have abundant common Pb (f206>2%).

Fig. 9. Cathodoluminescence (CL) images of selected zircons from LHGB metasedimentary rock sample 495628. Ages in Ma.

Fig. 10. Cathodoluminescence (CL) images of selected zircons from LHGB volcaniclastic rock sample 495643. Ages in Ma.

Fig. 11. Major and trace element plots for rocks of the Mulgathing Complex.

Fig. 12. Chondrite-normalized REE patterns for: a) Kenella Gneiss, b) Christie Gneiss, c) LHGB metasedimentary and volcaniclastic rocks and d) Glenloth Granite. Chondritic values from Taylor and McLennan (1985).

Fig. 13. $(La/Yb)_n$ vs. Ni (ppm) for rocks of the Mulgathing Complex. Chondritic values from Taylor and McLennan (1985).

Fig. 14. K-Na-Ca ternary diagram including the Glenloth Granite, typical late Archaean TTG's (Martin, 1994) and high-Ca granites of the Yilgarn Craton (Champion and Sheraton, 1997). Compositional similarities between the Glenloth Granite and other late Archaean TTG's suggest that subduction style tectonics may have existed in the late Archaean Mulgathing Complex.

Fig. 15. ε_{Nd} vs. age (Ma) as a function of crystallization or depositional age for Kenella Gneiss, Christie Gneiss, LHGB metasedimentary and volcaniclastic rocks and Glenloth Granite. Also plotted are the Devil's Playground Volcanics (*data from*: Cowley and Fanning, 1992).

Fig. 16. Rodinia reconstruction highlighting the correlation between the East Antarctic Shield and the Gawler Craton, southern Australia. U-Pb zircon ages (Ga) indicate the dominant provenance ages (*large numbers*) and metamorphic events (*small numbers*). (*Modified from*: Goodge *et al*., 2001).

Fig. 17. Primitive mantle normalized trace element diagram for the averaged available data for Archaean rhyodacite and andesite of the Devil's Playground Volcanics (*data from*: Cowley and Fanning, 1992) and the field for typical late Archaean arc-related felsic volcanics (*data from*: Dostal, 1997; Hollings and Wyman, 1999; Hollings *et al*., 1999; Wyman, 1999). The trace element signature of the Devil's Playground Volcanics, highlighted by depleted Nb and Ti anomalies suggests that they are subduction related arc-type volcanics. Data normalized to McDonough and Sun (1995).

Fig. 18. Primitive mantle normalized trace element diagram for LHGB komatiitic lavas (MER data, in prep) and the field for typical late Archaean komatiites from the Superior Province, Canada (*data from*: Hollings and Wyman, 1999; Hollings *et al*., 1999). Trace element data for the LHGB komatiites is consistent with a mantle-plume related origin. Data normalized to McDonough and Sun (1995).

Fig. 19. Tectonic model highlighting processes of crustal development of the late Archaean Gawler Craton. This model displays envisaged deposition of the protoliths to the Christie and Kenella gneisses in a shallow marine back-arc basin prior to eruption of the Devil's Playground Volcanics and LHGB mafic and ultramafic lavas between *ca*. 2510-2505 Ma. The model highlights (1) subduction related arc-style volcanism affiliated with the Devil's Playground Volcanics and (2) mantle-plume impingement resulting in rifting of the back-arc basin and extrusion of the LHGB mafic and ultramafic basalts and komatiites. Crustal thinning associated with high heat flow is consistent with an environment prone to metamorphism of extended duration such as the Sleafordian Orogeny (U-Pb zircon ages between *ca*. 2420 to 2500). Horizontal and vertical scales are schematic.

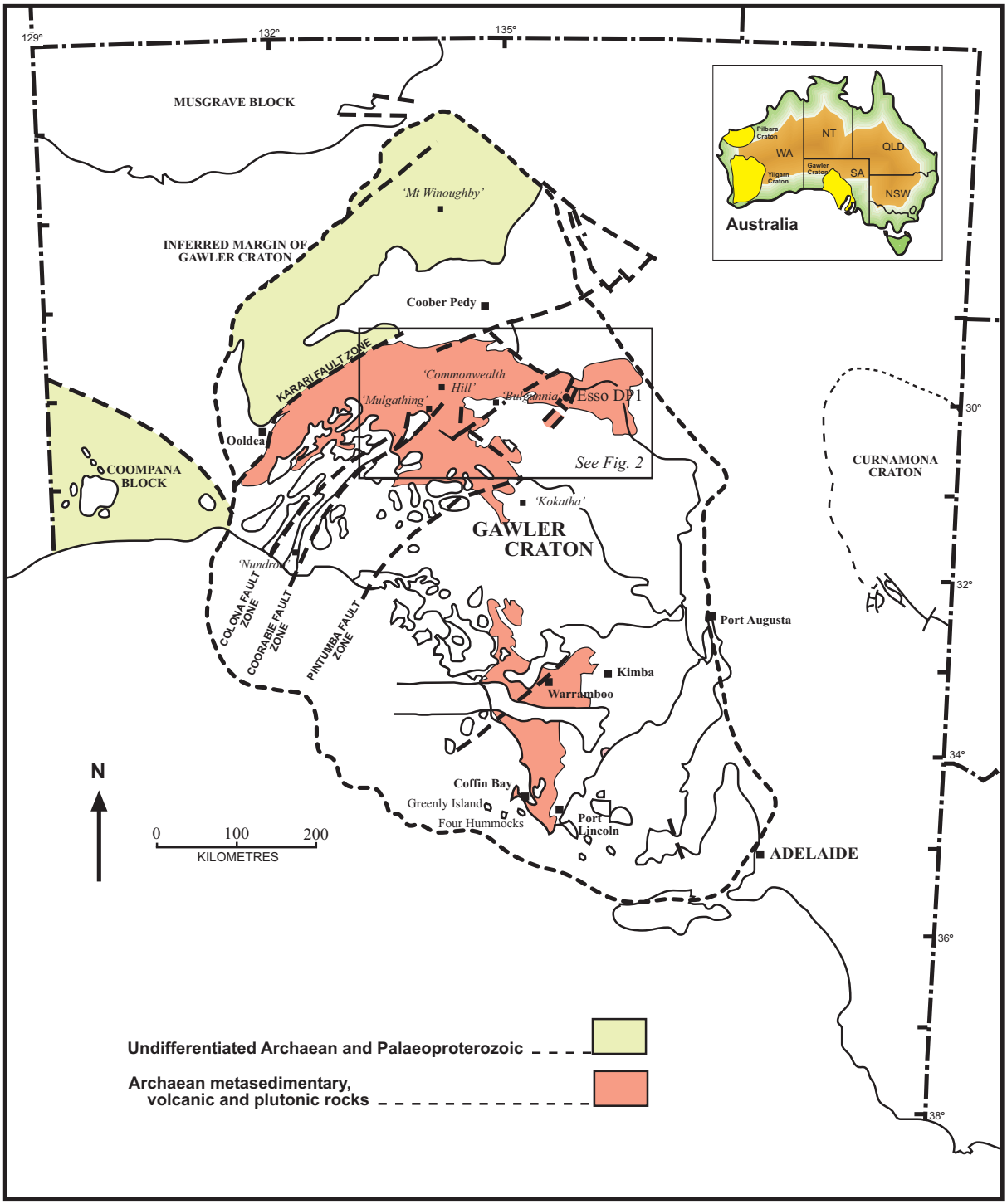

129°
132°
135°
30°
32°
34°
36°
38°
MUSGRAVE BLOCK
'Mt Winoughby'
INFERRED MARGIN OF GAWLER CRATON
Coober Pedy
KARARI FAULT ZONE
'Commonwealth Hill'
'Mulgathing'
'Bulgania'
Esso DP1
See Fig. 2
Ooldea
COOMPANA BLOCK
'Kokatha'
GAWLER CRATON
'Nundroo'
COLONA FAULT ZONE
COORABIE FAULT ZONE
PINTUMBA FAULT ZONE
CURNAMONA CRATON
Port Augusta
Kimba
Warramboo
Coffin Bay
Greenly Island
Four Hummocks
Port Lincoln
ADELAIDE
N
0 100 200
KILOMETRES
Undifferentiated Archaean and Palaeoproterozoic
Archaean metasedimentary, volcanic and plutonic rocks
Australia
Pilbara Craton
NT
WA
QLD
Gawler Craton
Yilgarn Craton
SA
NSW

Fig. 1

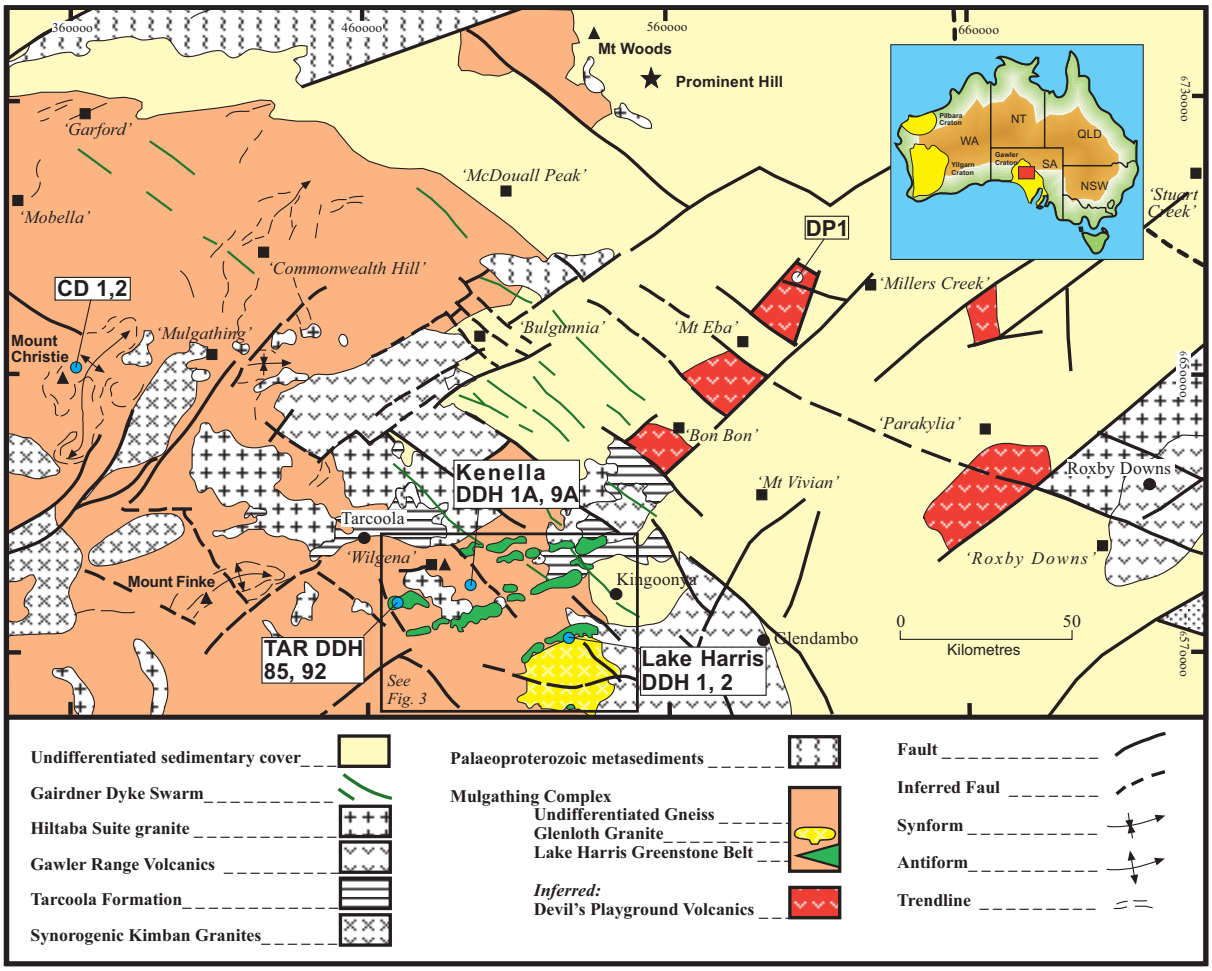

360000
460000
560000
660000
6730000
6650000
6570000
Mt Woods
Prominent Hill
'Garford'
'Mobella'
'McDouall Peak'
'Commonwealth Hill'
CD 1,2
Mount Christie
'Mulgathing'
'Bulgunnia'
'Mt Eba'
DP1
'Millers Creek'
'Stuart Creek'
'Bon Bon'
'Parakylia'
'Mt Vivian'
Roxby Downs
'Roxby Downs'
Kenella DDH 1A, 9A
Tarcoola
'Wilgena'
Mount Finke
Kingoonya
Glendambo
TAR DDH 85, 92
Lake Harris DDH 1, 2
See Fig. 3
0
50
Kilometres
NT
QLD
WA
SA
NSW
Pilbara Craton
Gawler Craton
Yilgarn Craton
Undifferentiated sedimentary cover
Gairdner Dyke Swarm
Hiltaba Suite granite
Gawler Range Volcanics
Tarcoola Formation
Synorogenic Kimban Granites
Palaeoproterozoic metasediments
Mulgathing Complex
Undifferentiated Gneiss
Glenloth Granite
Lake Harris Greenstone Belt
Inferred:
Devil's Playground Volcanics
Fault
Inferred Faul
Synform
Antiform
Trendline

Fig. 2

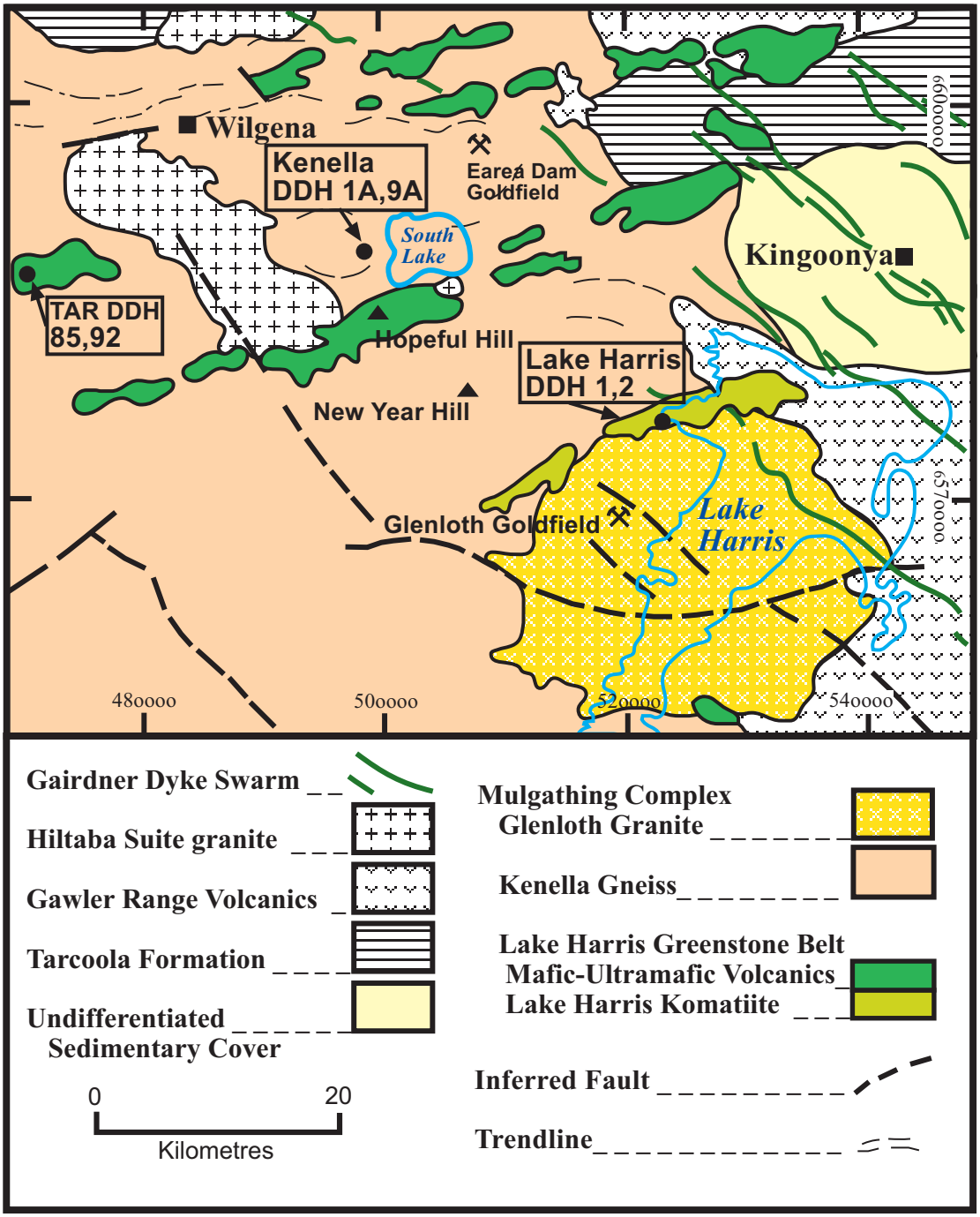

Wilgena
Kenella
DDH 1A,9A
Earea Dam
Goldfield
South
Lake
Kingoonya
TAR DDH
85,92
Hopeful Hill
Lake Harris
DDH 1,2
New Year Hill
Glenloth Goldfield
Lake
Harris
6600000
6570000
480000
500000
520000
540000
Gairdner Dyke Swarm
Hiltaba Suite granite
Gawler Range Volcanics
Tarcoola Formation
Undifferentiated
Sedimentary Cover
Mulgathing Complex
Glenloth Granite
Kenella Gneiss
Lake Harris Greenstone Belt
Mafic-Ultramafic Volcanics
Lake Harris Komatiite
Inferred Fault
Trendline
0
20
Kilometres

Fig. 3

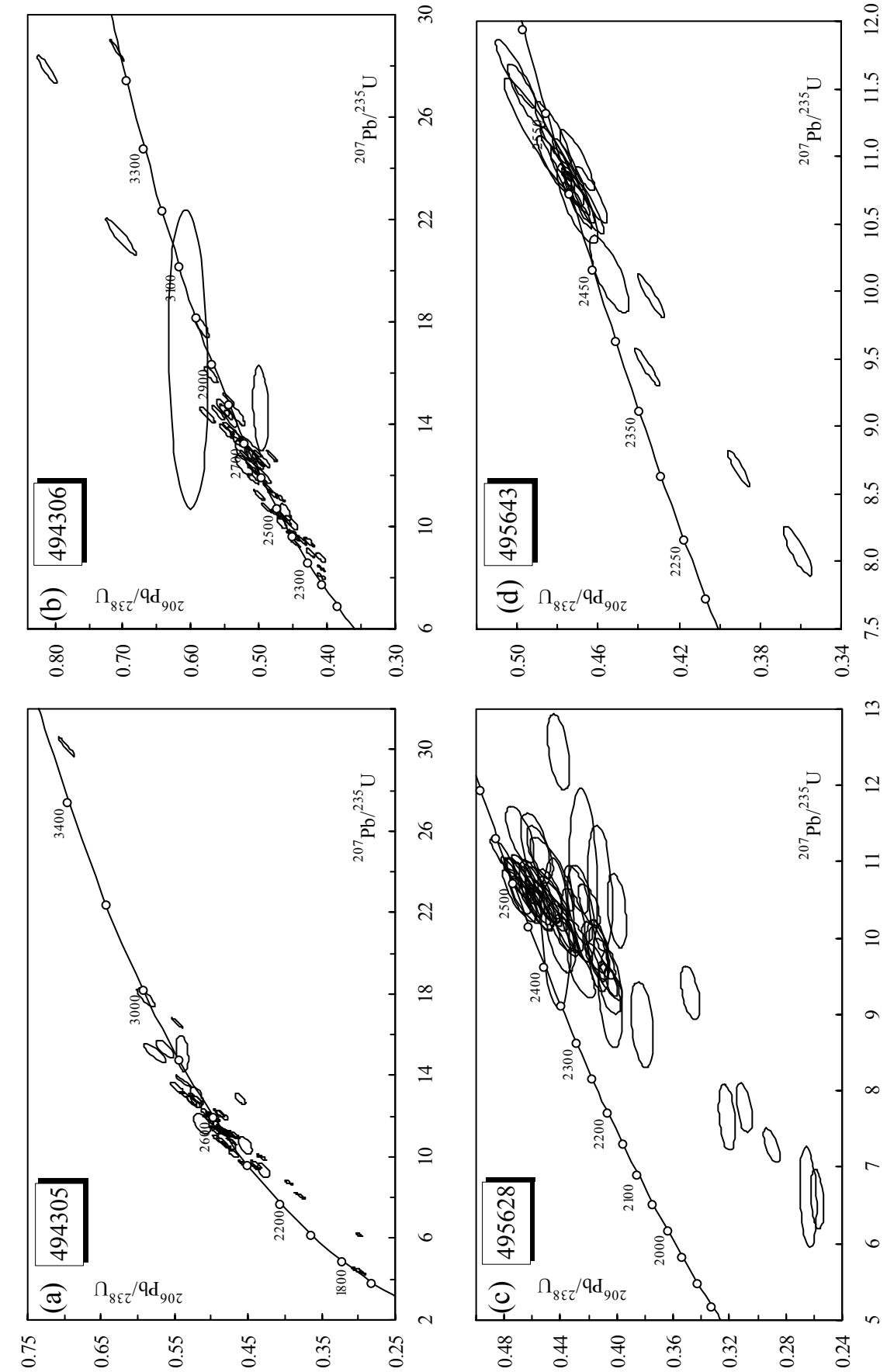


Fig. 4

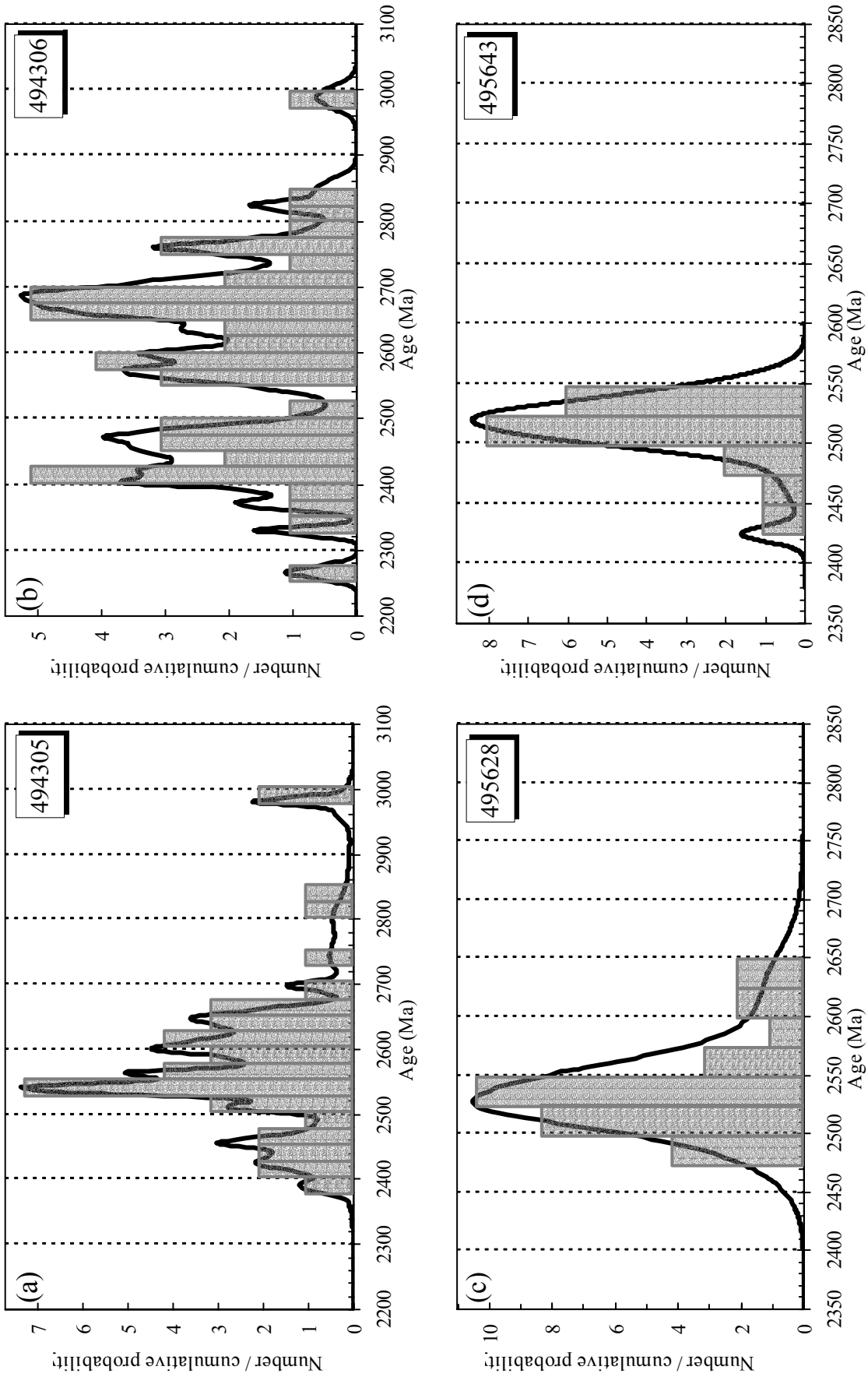

494306
(b)
494305
(a)
495643
(d)
495628
(c)
Number / cumulative probability
Age (Ma)

Fig. 5

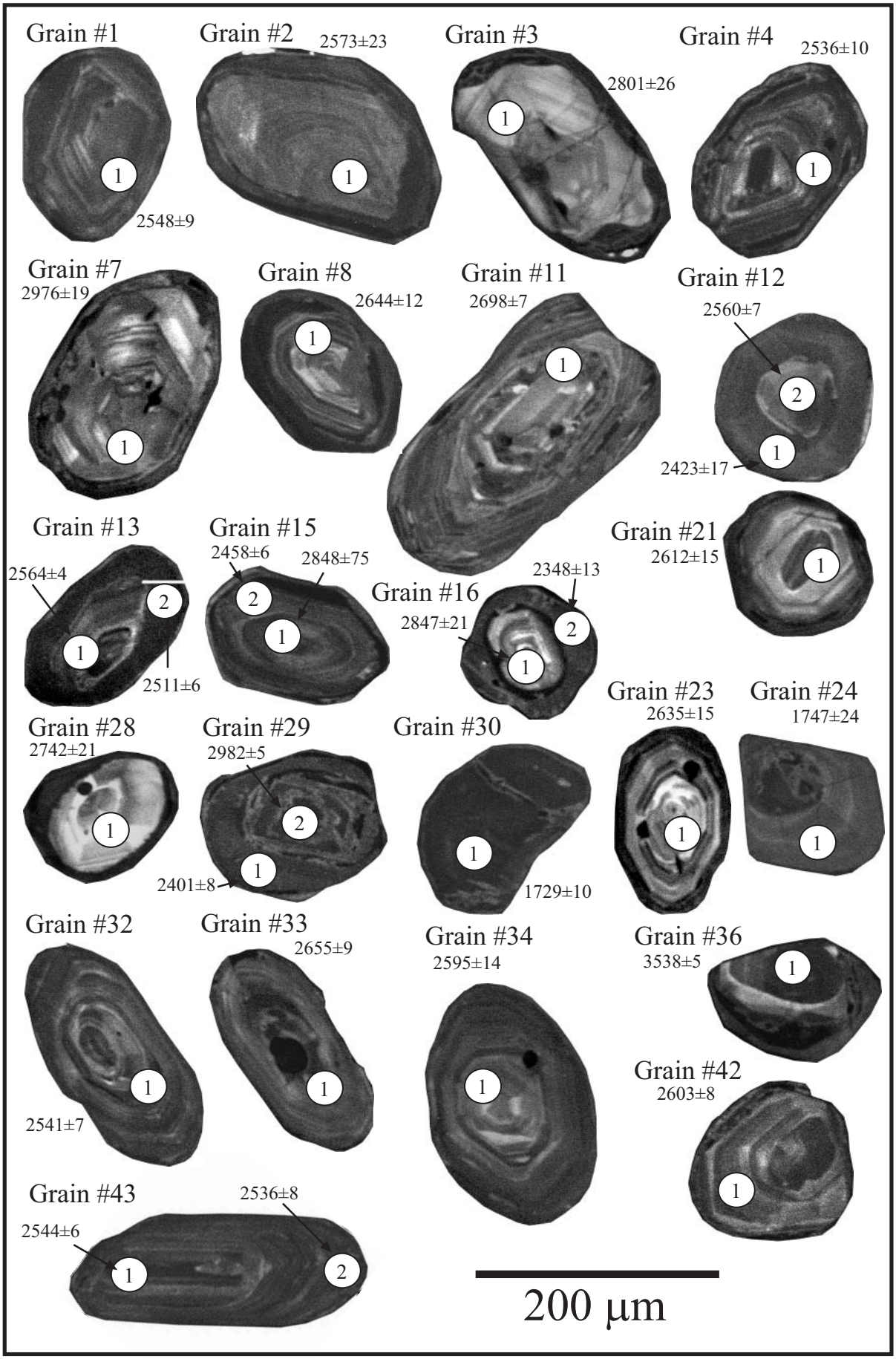

Grain #1
2548±9
Grain #2
2573±23
Grain #3
2801±26
Grain #4
2536±10
Grain #7
2976±19
Grain #8
2644±12
Grain #11
2698±7
Grain #12
2560±7
2423±17
Grain #13
2564±4
2511±6
Grain #15
2458±6
2848±75
Grain #16
2348±13
2847±21
Grain #21
2612±15
Grain #23
2635±15
Grain #24
1747±24
Grain #28
2742±21
Grain #29
2982±5
2401±8
Grain #30
1729±10
Grain #32
2541±7
Grain #33
2655±9
Grain #34
2595±14
Grain #36
3538±5
Grain #42
2603±8
Grain #43
2544±6
2536±8
200 μm

Fig. 6

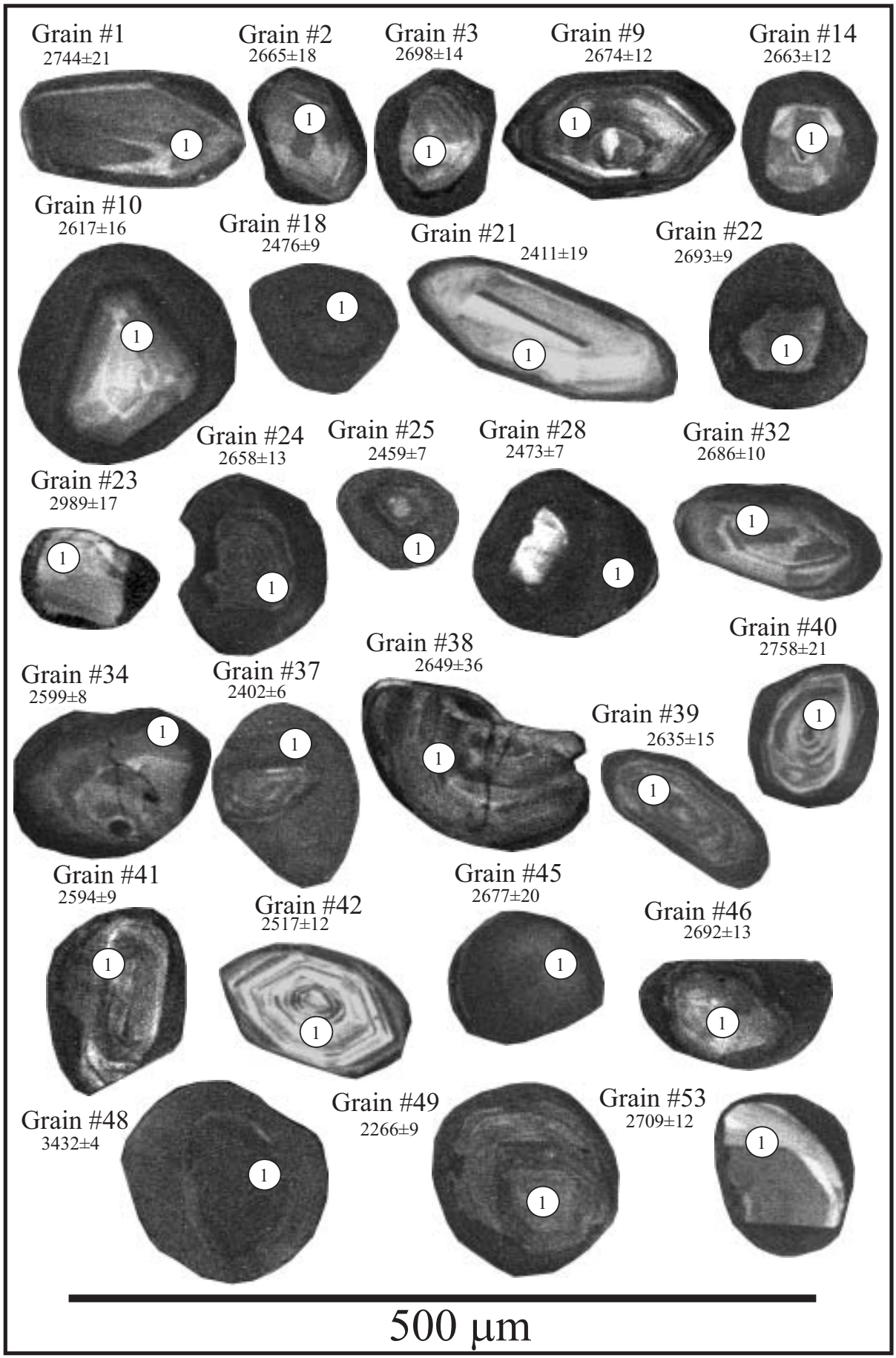

Grain #1
2744±21
Grain #2
2665±18
Grain #3
2698±14
Grain #9
2674±12
Grain #14
2663±12
Grain #10
2617±16
Grain #18
2476±9
Grain #21
2411±19
Grain #22
2693±9
Grain #24
2658±13
Grain #25
2459±7
Grain #28
2473±7
Grain #32
2686±10
Grain #23
2989±17
Grain #40
2758±21
Grain #38
2649±36
Grain #34
2599±8
Grain #37
2402±6
Grain #39
2635±15
Grain #41
2594±9
Grain #42
2517±12
Grain #45
2677±20
Grain #46
2692±13
Grain #48
3432±4
Grain #49
2266±9
Grain #53
2709±12
500 μm

Fig. 7

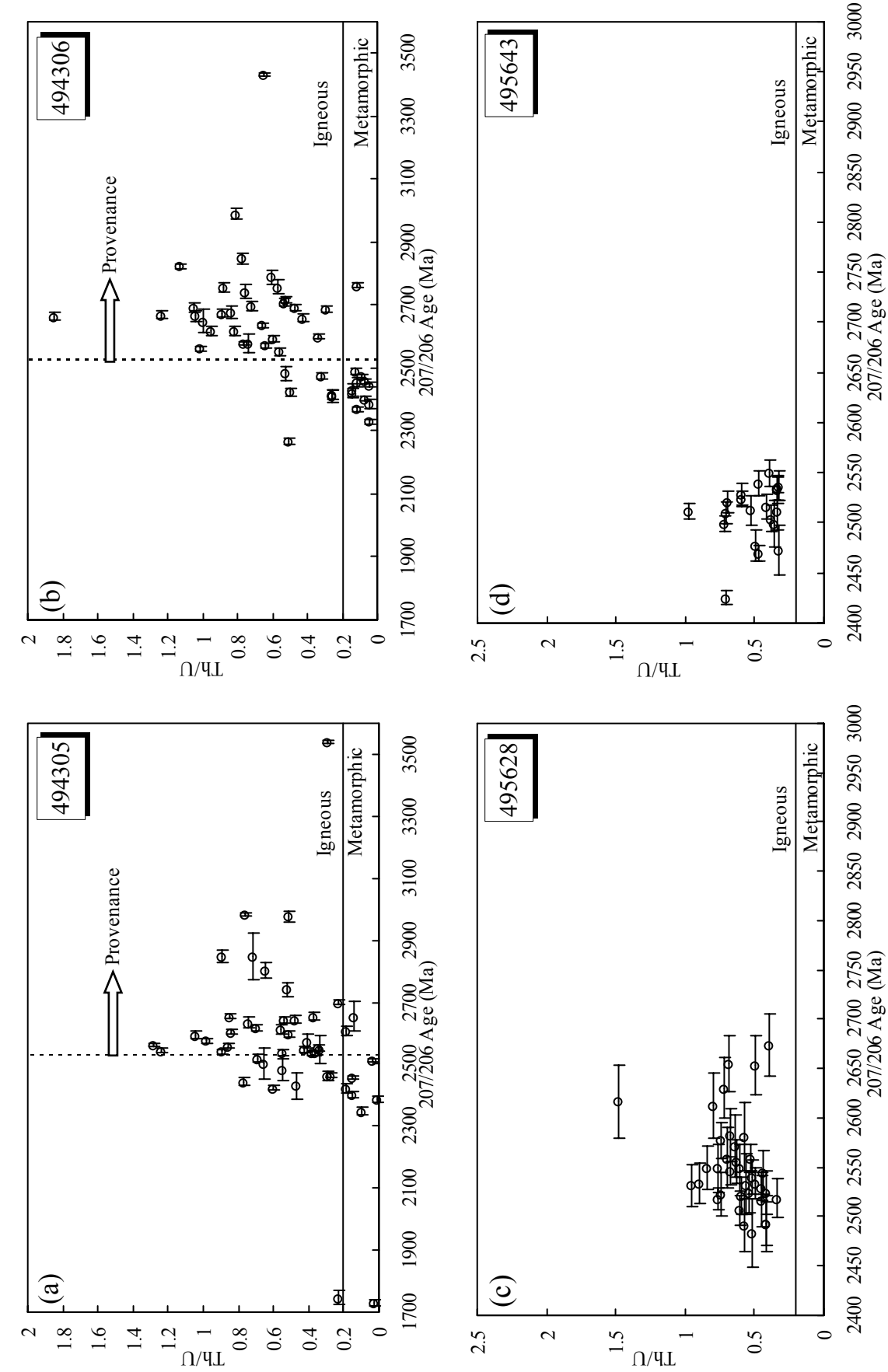

494306
(b)
Provenance
Igneous
Metamorphic
Th/U
207/206 Age (Ma)
495643
(d)
494305
(a)
495628
(c)

Fig. 8

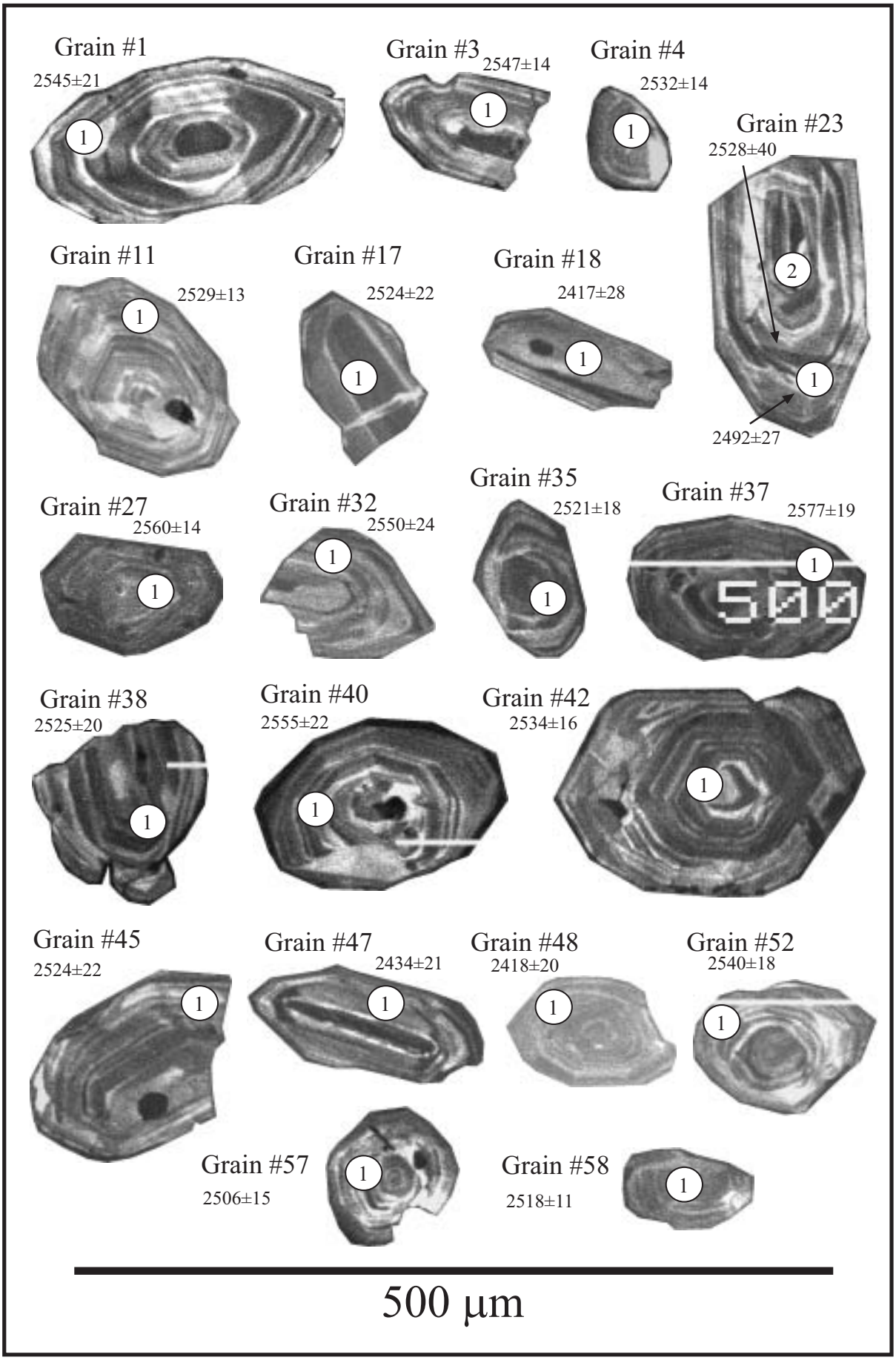

Grain #1
2545±21
Grain #3
2547±14
Grain #4
2532±14
Grain #23
2528±40
2492±27
Grain #11
2529±13
Grain #17
2524±22
Grain #18
2417±28
Grain #27
2560±14
Grain #32
2550±24
Grain #35
2521±18
Grain #37
2577±19
Grain #38
2525±20
Grain #40
2555±22
Grain #42
2534±16
Grain #45
2524±22
Grain #47
2434±21
Grain #48
2418±20
Grain #52
2540±18
Grain #57
2506±15
Grain #58
2518±11
500 µm

Fig. 9

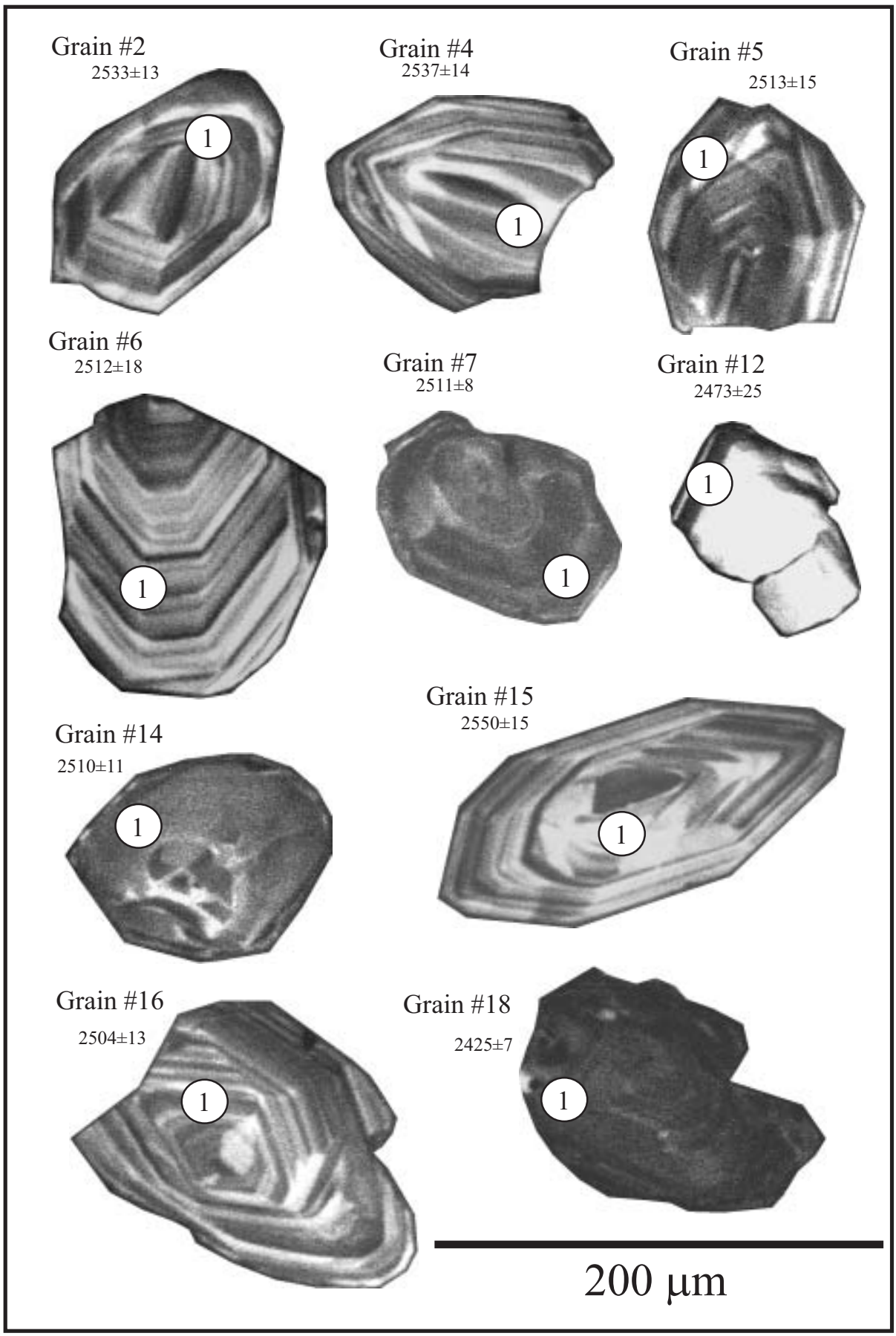

Grain #2
2533±13
Grain #4
2537±14
Grain #5
2513±15
Grain #6
2512±18
Grain #7
2511±8
Grain #12
2473±25
Grain #14
2510±11
Grain #15
2550±15
Grain #16
2504±13
Grain #18
2425±7
200 μm

Fig. 10

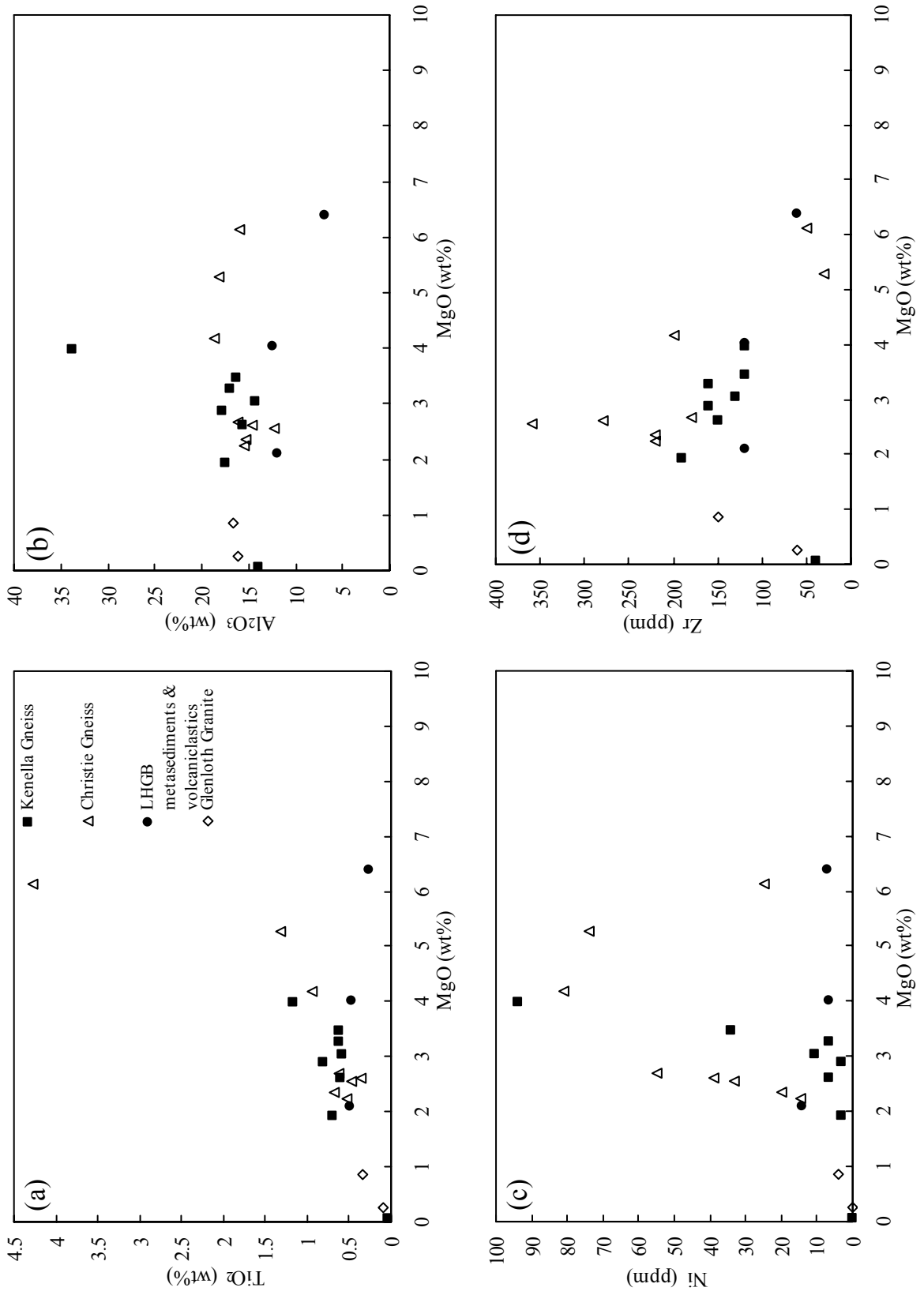

(a)
TiO2 (wt%)
MgO (wt%)
Kenella Gneiss
Christie Gneiss
LHGB metasediments & volcaniclastics
Glenloth Granite
(b)
Al2O3 (wt%)
MgO (wt%)
(c)
Ni (ppm)
MgO (wt%)
(d)
Zr (ppm)
MgO (wt%)

Fig. 11

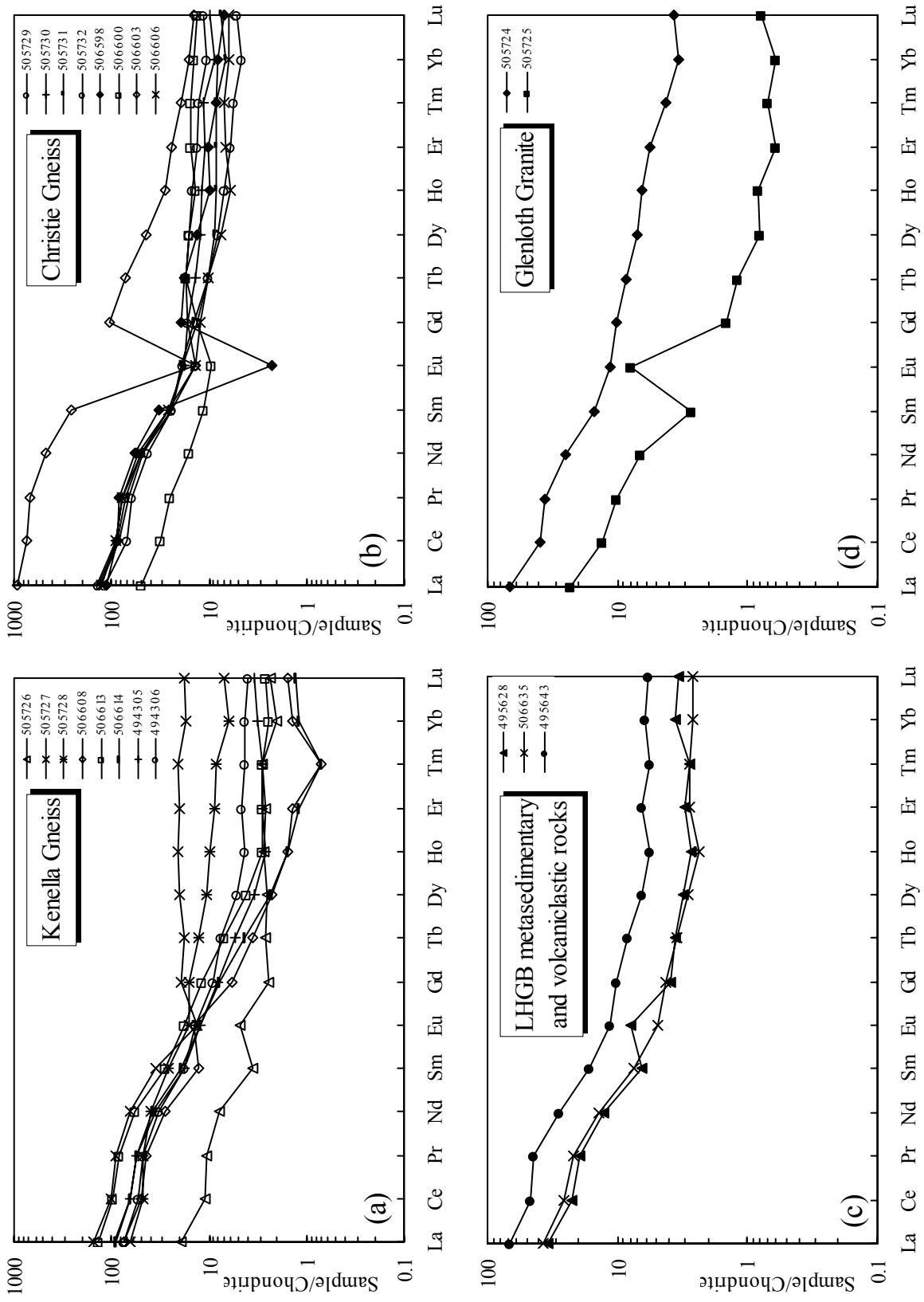

Kenella Gneiss
505726
505727
505728
506608
506613
506614
494305
494306
(a)
Christie Gneiss
505729
505730
505731
505732
506598
506600
506603
506606
(b)
LHGB metasedimentary and volcaniclastic rocks
495628
506635
495643
(c)
Glenloth Granite
505724
505725
(d)
Sample/Chondrite
1000
100
10
1
0.1
La Ce Pr Nd Sm Eu Gd Tb Dy Ho Er Tm Yb Lu

Fig. 12

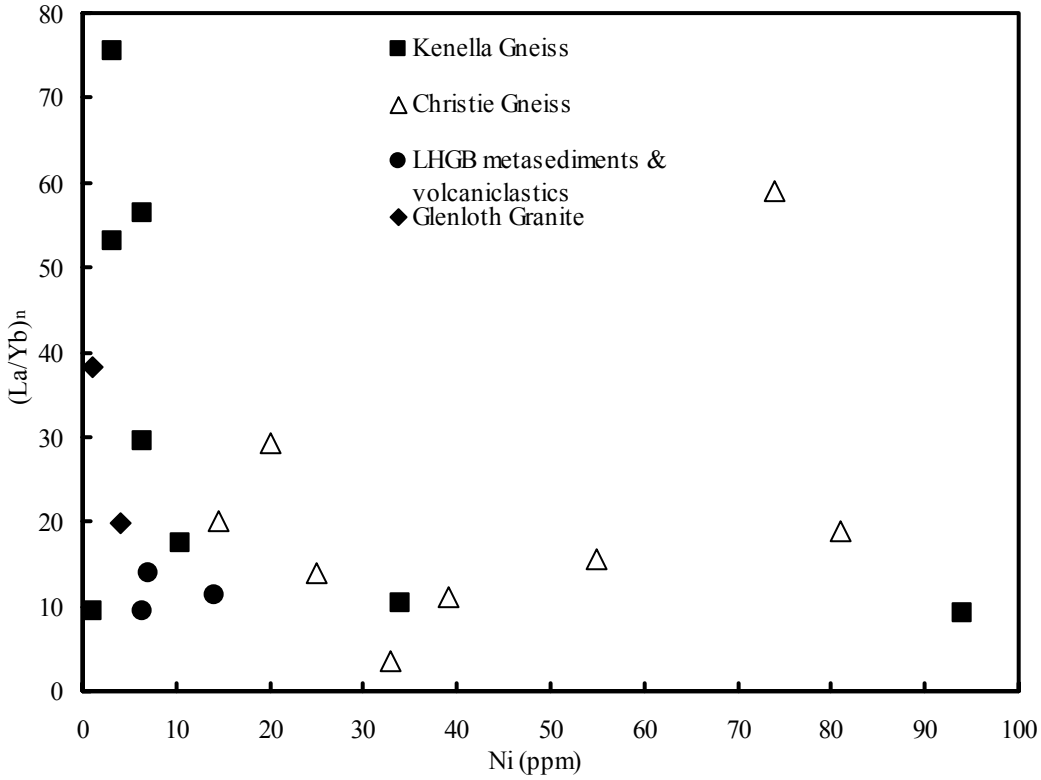

Kenella Gneiss
Christie Gneiss
LHGB metasediments & volcaniclastics
Glenloth Granite
(La/Yb)n
Ni (ppm)
0
10
20
30
40
50
60
70
80
90
100

Fig. 13

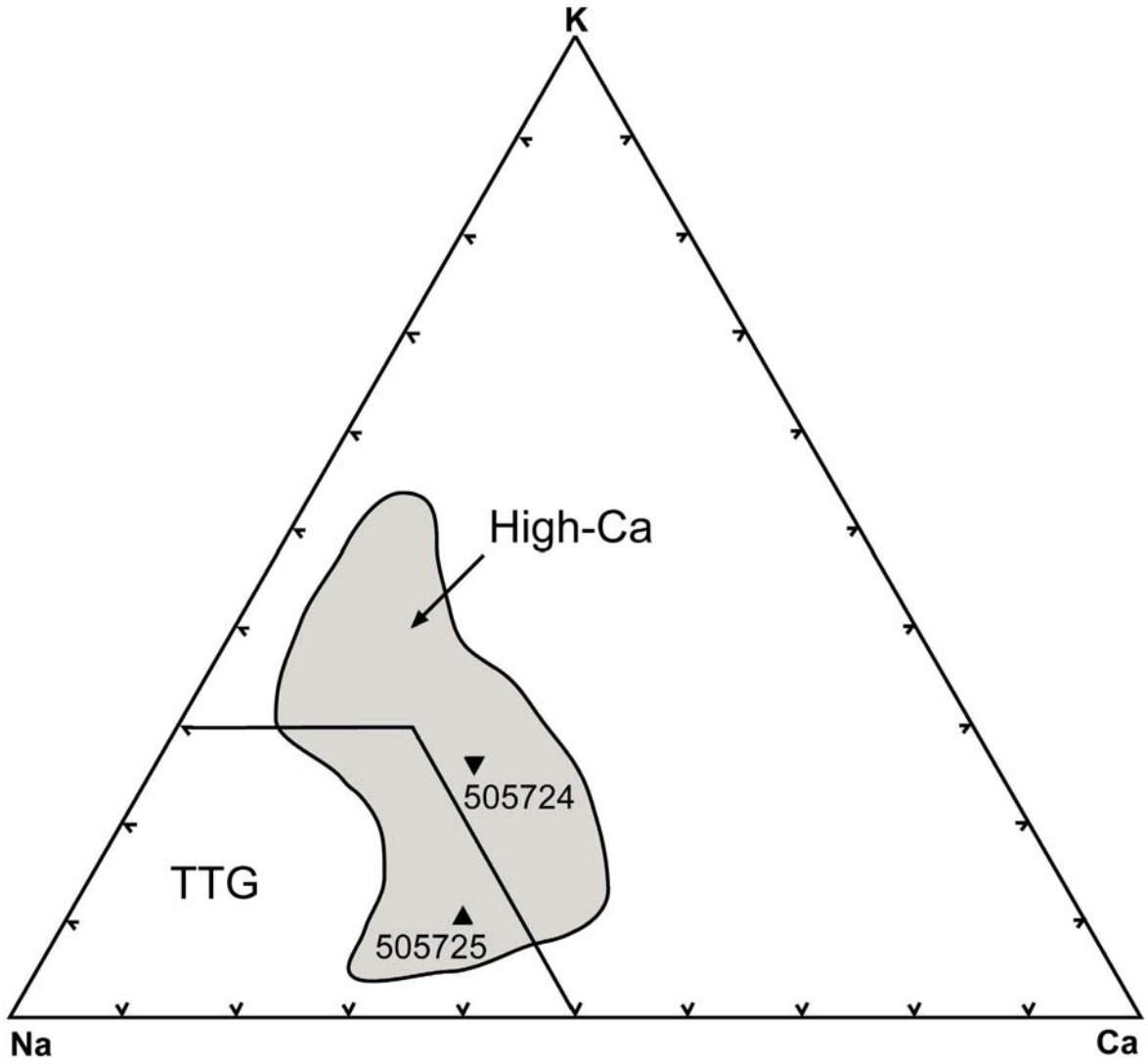


Fig. 14

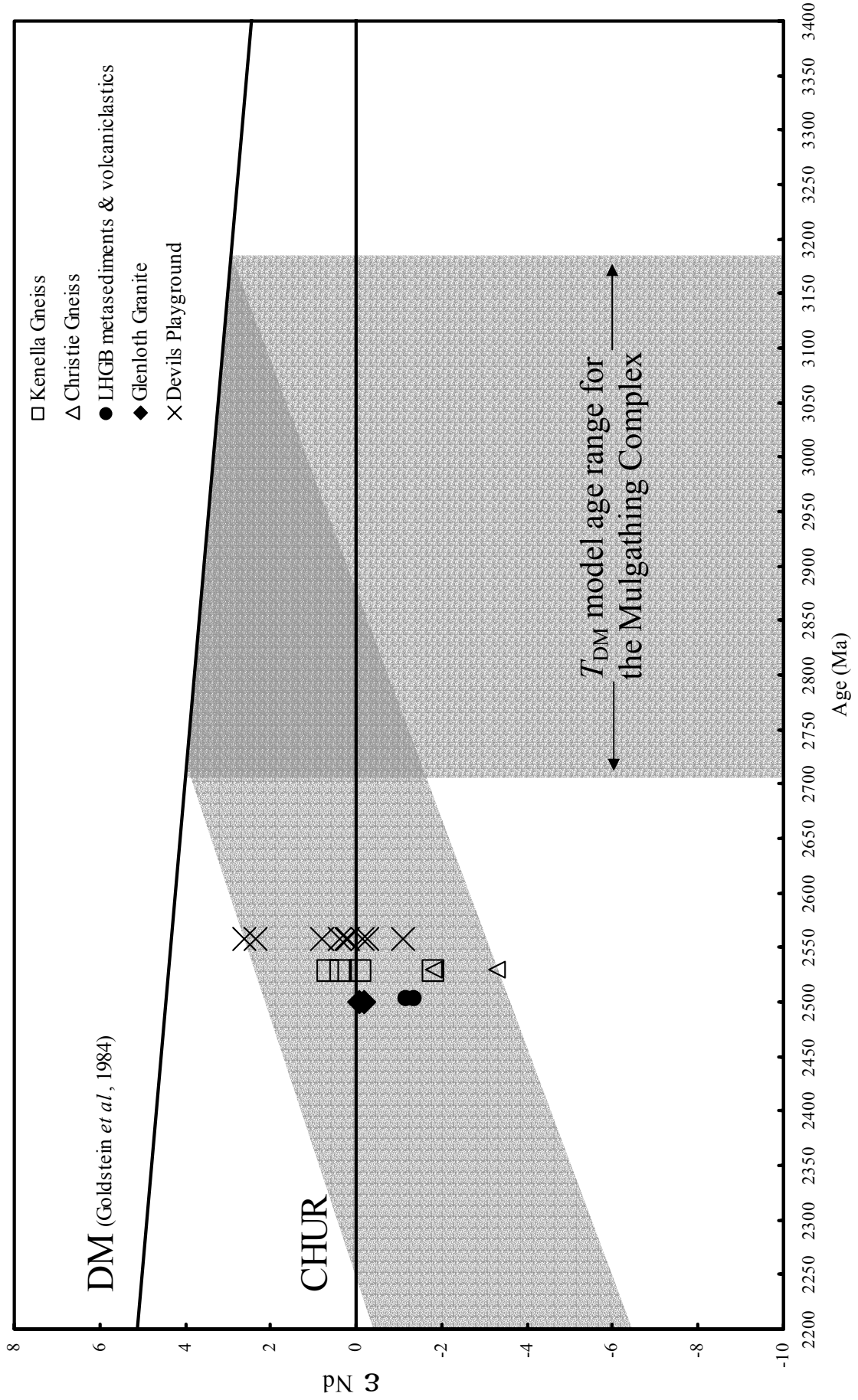

□ Kenella Gneiss
△ Christie Gneiss
● LHGB metasediments & volcaniclastics
◆ Glenloth Granite
× Devils Playground
DM (Goldstein *et al*, 1984)
CHUR
T_{DM} model age range for the Mulgathing Complex
εNd
Age (Ma)
8
6
4
2
0
-2
-4
-6
-8
-10
2200 2250 2300 2350 2400 2450 2500 2550 2600 2650 2700 2750 2800 2850 2900 2950 3000 3050 3100 3150 3200 3250 3300 3350 3400

Fig. 15

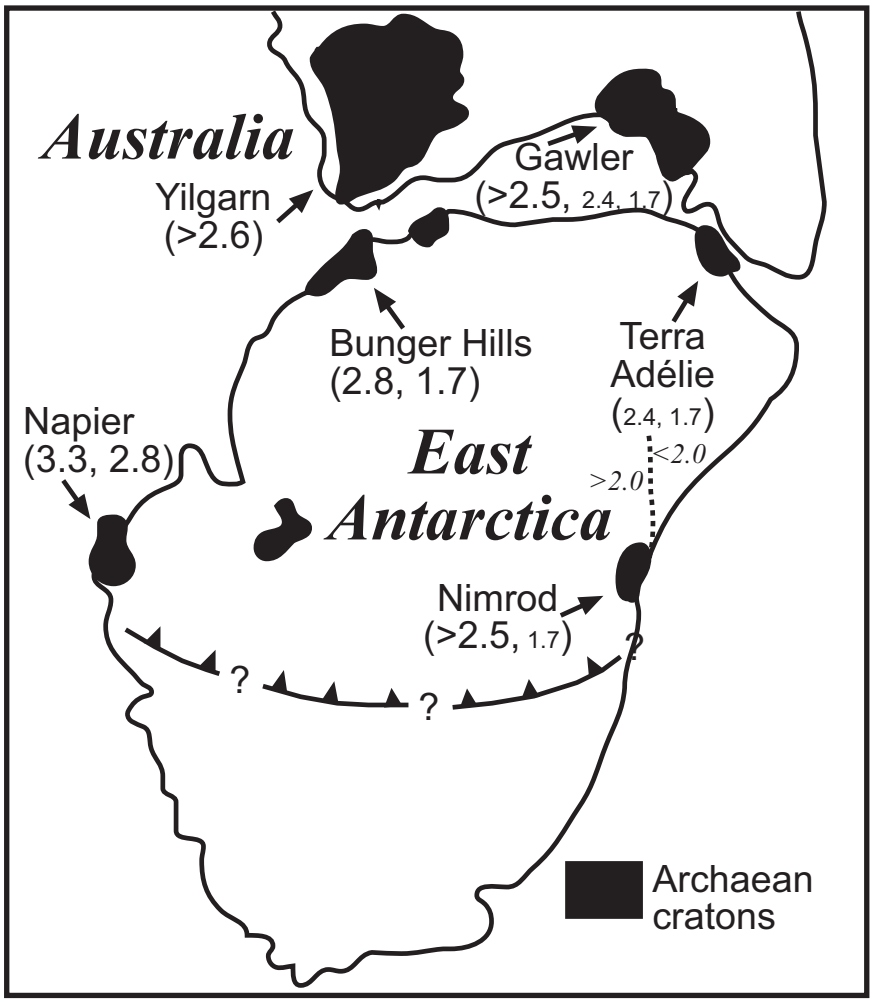

Australia
Yilgarn
(>2.6)
Gawler
(>2.5, 2.4, 1.7)
Bunger Hills
(2.8, 1.7)
Terra
Adélie
(2.4, 1.7)
Napier
(3.3, 2.8)
East
Antarctica
<2.0
>2.0
Nimrod
(>2.5, 1.7)
?
?
?
Archaean
cratons

Fig. 16

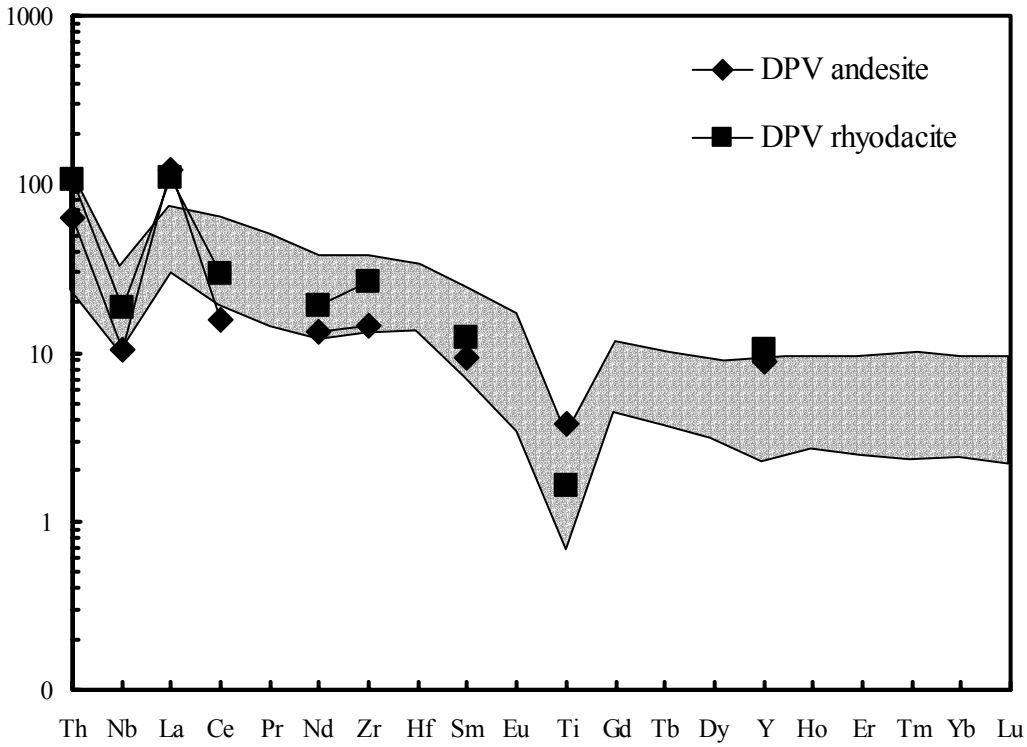

1000
100
10
1
0
DPV andesite
DPV rhyodacite
Th Nb La Ce Pr Nd Zr Hf Sm Eu Ti Gd Tb Dy Y Ho Er Tm Yb Lu

Fig. 17

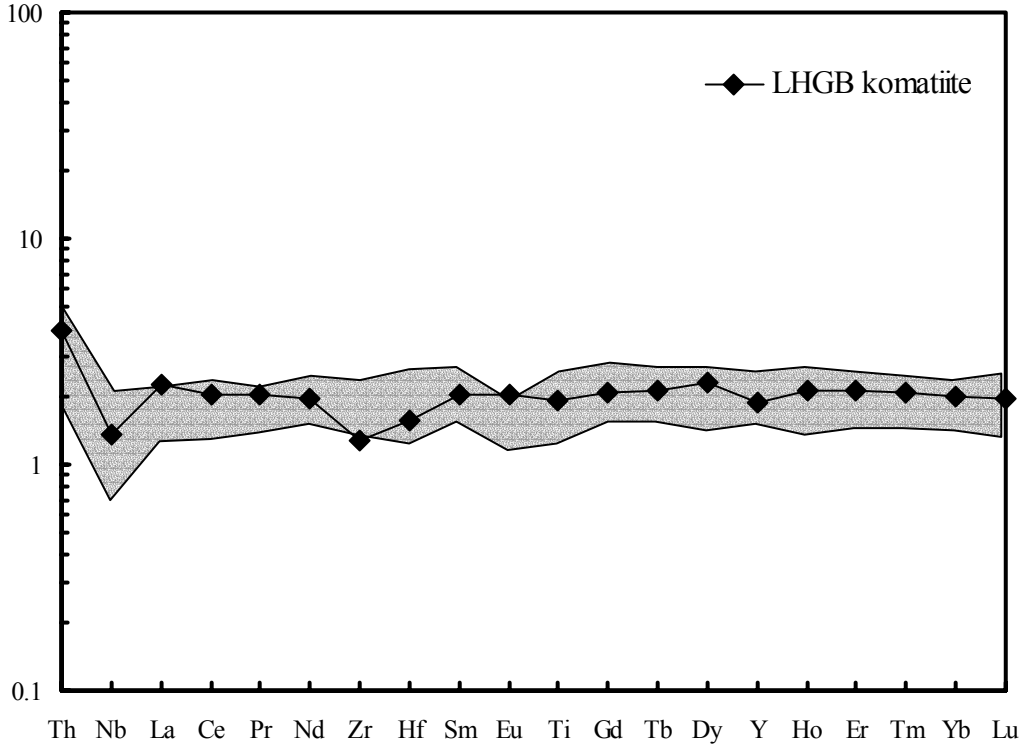

100
10
1
0.1
LHGB komatiite
Th Nb La Ce Pr Nd Zr Hf Sm Eu Ti Gd Tb Dy Y Ho Er Tm Yb Lu

Fig. 18

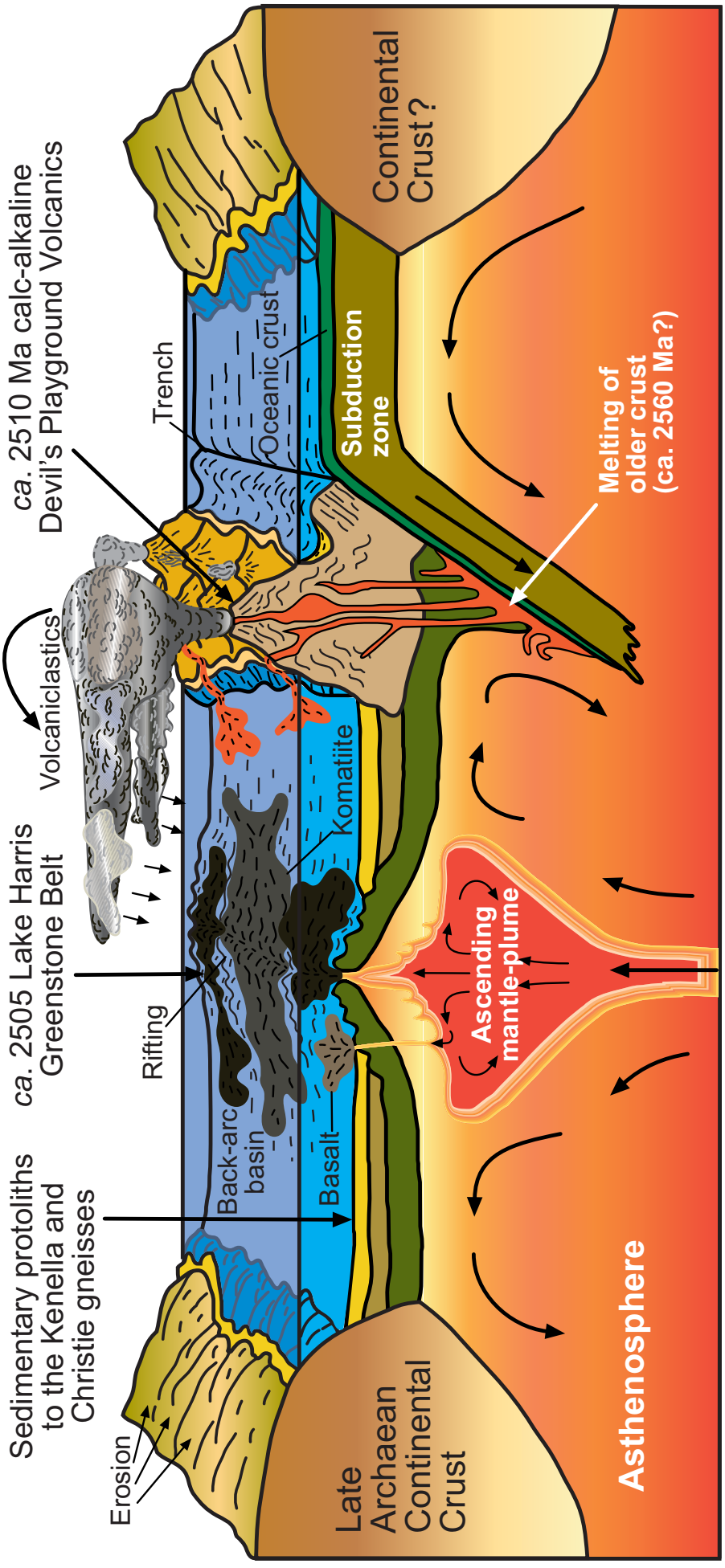

Continental Crust ?
ca. 2510 Ma calc-alkaline Devil's Playground Volcanics
Trench
Oceanic crust
Subduction zone
Melting of older crust (ca. 2560 Ma?)
Volcaniclastics
ca. 2505 Lake Harris Greenstone Belt
Komatiite
Rifting
Ascending mantle-plume
Sedimentary protoliths to the Kenella and Christie gneisses
Back-arc basin
Basalt
Erosion
Late Archaean Continental Crust
Asthenosphere

Fig. 19